Phys Chem Minerals (2007) 34:409–430
DOI 10.1007/s00269-007-0158-6

ORIGINAL PAPER

# Fe–Mg diffusion in olivine II: point defect chemistry, change of diffusion mechanisms and a model for calculation of diffusion coefficients in natural olivine

**Ralf Dohmen · Sumit Chakraborty**

Received: 4 October 2006 / Accepted: 19 March 2007 / Published online: 23 May 2007


**Abstract** Analysis of existing data and models on point defects in pure (Fe,Mg)-olivine (Phys Chem Miner 10:27–37,1983; Phys Chem Miner 29:680–694, 2002) shows that it is necessary to consider thermodynamic non-ideality of mixing to adequately describe the concentration of point defects over the range of measurement. In spite of different sources of uncertainties, the concentrations of vacancies in octahedral sites in (Fe,Mg)-olivine are on the order of $10^{-4}$ per atomic formula unit at 1,000–1,200 °C according to both the studies. We provide the first explicit plots of vacancy concentrations in olivine as a function of temperature and oxygen fugacity according to the two models. It is found that in contrast to absolute concentrations at ~1,100 °C and dependence on $fO_2$, there is considerable uncertainty in our knowledge of temperature dependence of vacancy concentrations. This needs to be considered in discussing the transport properties such as diffusion coefficients. Moreover, these defect models in pure (Fe,Mg)-olivine need to be extended by considering aliovalent impurities such as Al, Cr to describe the behavior of natural olivine. We have developed such a formulation, and used it to analyze the considerable database of diffusion coefficients in olivine from Dohmen et al. (Phys Chem Miner this volume, 2007) (Part - I) and older data in the literature. The analysis documents unequivocally for the first time a change of diffusion mechanism in a silicate mineral—from the transition metal extrinsic (TaMED) to the purely extrinsic (PED) domain, at $fO_2$ below $10^{-10}$ Pa, and consequently, temperatures below 900 °C. The change of diffusion mechanism manifests itself in a change in $fO_2$ dependence of diffusivity and a slight change in activation energy of diffusion—the activation energy *increases* at lower temperatures. These are consistent with the predictions of Chakraborty (J Geophys Res 102(B6):12317–12331, 1997). Defect formation enthalpies in the TaMED regime (distinct from intrinsic defect formation) lie between –66 and + 15 kJ/mol and migration energies of octahedral cations in olivine are most likely ~ 260 kJ/mol, consistent with previous inferences (Phys Chem 207:147–162, 1998). Plots are shown for diffusion at various constant $fO_2$ as well as along $fO_2$ buffers, to highlight the difference in behavior between the two. Considering all the diffusion data and constraints from the point defect models, (Fe–Mg) diffusion in olivine along [001] is best described by the Master equations: (1) At oxygen fugacities greater than $10^{-10}$ Pa:

$$\log[D_{\mathrm{FeMg}}(m^2/s)] = -9.21 - \frac{201000 + (P - 10^5) \times 7 \times 10^{-6}}{2.303RT} + \frac{1}{6}\log(fO_2/10^{-7}) + 3X_{\mathrm{Fe}}$$

where $T$ is in Kelvin, $P$ and $fO_2$ is in Pascals, $X_{\mathrm{Fe}}$ is the mole fraction of the fayalite component and $R$ is the gas constant in J/mol/K. (2) At oxygen fugacities less than $10^{-10}$ Pa:

$$\log[D_{\mathrm{FeMg}}(m^2/s)] = -8.91 - \frac{220000 + (P - 10^5) \times 7 \times 10^{-6}}{2.303RT} + 3X_{\mathrm{Fe}}$$

These equations reproduce all of the 113 experimental data points within half an order of magnitude. (3) Alternately, a global equation averaging out the change of mechanism

R. Dohmen (✉) · S. Chakraborty
Institut für Geologie, Mineralogie und Geophysik,
Ruhr Universität Bochum, 44780 Bochum, Germany
e-mail: ralf.dohmen@rub.de

may be used, with somewhat larger errors in reproducing the measured diffusion data. It underestimates data at higher temperatures, and overestimates them at lower temperatures on the average. Note that $fO_2$ is not explicitly considered here, leading to additional sources of error:

$$\log[D_{\mathrm{FeMg}}(m^2/s)] = -8.27 - \frac{226000 + (P - 10^5) \times 7 \times 10^{-6}}{2.303RT} + 3X_{\mathrm{Fe}}$$

To obtain diffusion coefficients along [100] and [010], log 6 needs to be subtracted from each of the above equations.

**Keywords** Olivine · Point defect · Thermodynamics · Diffusion mechanism · Intrinsic · Extrinsic · Trace elements

## List of Symbols

### Structural units of olivine (in Kröger–Vink notation)

| | |
|---|---|
| $Mg_{Me}^{x}$ | $Mg^{2+}$ on a metal site |
| $Mg_{i}^{\cdot\cdot}$ | $Mg^{2+}$ on an interstitial site |
| $Fe_{Me}^{x}$ | $Fe^{2+}$ on a metal site |
| $Si_{Si}^{x}$ | $Si^{4+}$ on a Si site |
| $V_{Me}^{\cdot\cdot}$ | vacancy on a metal site |
| $Fe_{Me}^{\bullet}$ | $Fe^{3+}$ on a metal site |
| $Fe_{Si}^{\cdot\cdot}$ | $Fe^{3+}$ on a Si site |
| $\{Fe_{Me}^{\bullet}Fe_{Si}^{\prime}\}$ | association of $Fe^{3+}$ on the metal site with those on the Si site |
| $V_{Si}^{''''}$ | vacancy on a Si site |
| $O_{i}^{\bullet\bullet}$ | $O^{2-}$ on an interstitial site |
| $Al_{Si}^{\prime}$ | $Al^{3+}$ on a Si site |
| $Al_{Me}^{\bullet}$ | $Al^{3+}$ on a metal site |
| $Cr_{Me}^{\bullet}$ | $Cr^{3+}$ on a metal site |
| $OH_{O}^{\bullet}$ | hydroxyl group, $OH^{-}$, on an oxygen site |

### Thermodynamic variables

| | |
|---|---|
| $P$ | pressure |
| $T$ | temperature |
| $R$ | universal gas constant |
| $fO_2$ | oxygen fugacity |
| $\mu_j$ | chemical potential of chemical component or structural unit j in olivine |
| $\mu_j^0$ | chemical potential of chemical component or structural unit j in the reference state<br>Note that the reference state for all structural units in this work is chosen to be pure stoichiometric fayalite, $Fe_2SiO_4$ |
| $a$(j) or $a_j$ | activity of chemical component or structural unit j in olivine |
| $K_i$ | equilibrium constant of reaction $i$ |
| $K_{\gamma(i)}$ | product term with the activity coefficients from the mass action law of reaction $i$ |
| $K_{x(i)} = K_i/K_{\gamma(i)}$ | Compositional part of the equilibrium constant, also described as ''equilibrium constant'' in this work, of reaction $i$ |
| $W_{ij}$ | binary interaction parameter of structural unit i and j for a model of mixing on the metal site |
| $C_{ijk}$ | ternary interaction parameter for the model of mixing on the metal site |

### Diffusion variables

| | |
|---|---|
| $D_{Fe}^{*}$, $D_{Mg}^{*}$ | Self diffusion coefficients of Fe and Mg, respectively |
| $D_{(Fe-Mg)}$ | interdiffusion coefficient of Fe and Mg |
| $f_{Mg}$, $f_{Fe}$ | geometrical correlation factors for Fe and Mg diffusion, respectively |
| $\Gamma_{Fe}$, $\Gamma_{Mg}$ | jump frequency of Fe and Mg self diffusion, respectively |
| $\lambda$ | jump distance for diffusion on the metal site |
| $\Delta H_f$ | formation enthalpy of metal vacancies |
| $\Delta \bar{H}_m$ | averaged migration energy for vacancy diffusion on the metal site |

### Compositional variables

| | |
|---|---|
| [$j$] | concentration of element or structural unit j in olivine in units of number per formula unit of $M_2SiO_4$ |
| $X_{Fe}$ | [Fe]/([Fe] + [Mg]), molar fraction of Fe on the metal site ignoring effects of point defects and impurities |
| $\xi$ | [Si]/([Si] + [Fe] + [Mg]) (see also Eq. 8) |
| $[IP_{Me}^{\bullet}]$ | excess concentration of trivalent impurities on the metal site, defined in Eq. 20 |

## Introduction

Fe–Mg diffusion coefficients in olivine are now available at a wide range of conditions (see Dohmen et al. 2007 hereafter referred to as Part I, for new as well as a review of existing data) and the dataset reveals some enigmatic features. Understanding the data set and its application in diverse pressure, temperature, composition and oxygen fugacity conditions in natural systems requires it to be based on an understanding of diffusion mechanisms and point defect chemistry. The nature and concentration of point defects in pure, synthetic (Fe,Mg)-olivine have been studied by Nakamura and Schmalzried (1983, referred to as NS83 hereafter) and Tsai and Dieckmann (2002, referred to

as TD02 hereafter). Simons (1986) studied the temperature dependence of these defects in pure fayalite and Hillert et al. (1996) re-analyzed the experimental data of Nakamura and Schmalzried (1983) using new thermodynamic data to obtain a modified stability field of fayalite as a function of point defect concentrations. The main difference between the data of NS83 and TD02 result from differences in experimental protocol (e.g., use/avoidance of Pt capsules and wires). It is important to recognize that the quantities directly measured in their experiments are not point defect concentrations—these are inferred based on thermodynamic analysis of the results of their thermogravimetric experiments. There are important differences in the assumptions underlying the thermodynamic analysis of these two studies as well. One of the limitations of the available results is that data has been collected over a very limited temperature range (mostly 1,130–1,200 °C). Yet, it is the temperature dependence of defect concentrations that is central to the understanding of many diffusion related properties (e.g., activation energies). In the first part of this work, we have carried out an analysis of the experimental approach and thermodynamic approximations underlying the two works. In the process, we present the first explicit plots of vacancy concentrations as a function of temperature and $fO_2$ in these olivines which allow the difference between the expected diffusion behavior according to results from the two studies to be clearly outlined. The objective is to evaluate the point defect data/models as well as the diffusion data presented in Part I to obtain a consistent picture.

Notwithstanding the experimental challenge in carrying out the measurements reported in NS83 and TD02, the data do not completely represent the situation for natural olivines that always contain a variety of trace elements (e.g., Ni, Mn, Cr, Al, Ti, H, P). Other than for the rather specialized case of H (Kohlstedt and Mackwell 1998; Hier-Majumder et al. 2005), the role of these trace elements in affecting the point defect chemistry and hence transport behavior (diffusion, electrical conductivity, creep) in ferromagnesian olivine has not yet been studied. In the second part of the paper we extend our analysis to obtain an integrated model that formally incorporates the role of impurities in controlling point defect chemistry. This integrated analysis enables us to characterize diffusion behavior over a wide range of temperature and $fO_2$ spanning the entire stability field of olivine and helps us to explain some enigmatic observations from Part I. In the process, we are able to locate quantitatively a change in diffusion mechanism (expressed through variations in temperature and $fO_2$ dependence of diffusion rates) from the TaMED to the PED mechanism in olivine, as predicted by Chakraborty (1997) for diffusion in Fe-bearing silicates [See Appendix A and Chakraborty 1997, for definitions of these acronyms].

In the last section, we combine the recently developed large diffusion database with the analysis of point defect concentrations as a function of temperature and oxygen fugacity to obtain an internally consistent formulation that allows one to calculate diffusion coefficients (primarily Fe–Mg, but by inference also for divalent cations such as Ni and Mn, see Petry et al. 2004; Holzapfel et al. 2007) as a function of $T$, $fO_2$, $P$ and composition (Fe/Mg ratio, trace element concentrations) of olivines over their entire stability field in the temperature range of 600–1,300 °C.

## Point defect chemistry of olivine

### Basic concepts and conventions used in this paper

The basic premise of point defect thermodynamics is that all *structural units* of a single crystal, regular structural units as well as point defects, can be treated as quasi-chemical species. To denote the structural units ($\alpha$) of a single crystal the Kröger–Vink notation is used, whereby $\alpha \equiv X_y^z$, where X ≡ Species, i.e., element/defect (V: vacancy, I: interstitial), y ≡ crystallographic site (e.g., Me for an octahedral metal site or i for interstitial) and $z$ ≡ effective charge relative to the ideal crystal. The conventional symbols for z are as follows: a cross ($^x$) indicates no excess/deficit charge relative to ideal crystal (e.g., a $Fe^{2+}$ in the octahedral metal site of olivine), a dash ($'$) indicates an effective negative/a missing positive charge (e.g., an electron or a monovalent cation vacancy) and a dot ($^\bullet$) indicates an effective positive/missing negative charge (e.g., $Fe^{3+}$ in an octahedral metal site in olivine, or a monovalent anion vacancy). Multiple charges are indicated by simply repeating the dot or dash the required number of times, as will be seen in examples below. To denote concentrations of the regular structural units, we use parentheses []. For example, $[V''_{Me}]$ is the number of vacancy structural units per formula unit of olivine ($Me_2SiO_4$). Each structural unit $\alpha$ is assigned a chemical potential, $\mu_\alpha$ which cannot, however, be measured independently. Only neutral combinations of them, so-called *building blocks*, have a defined, measurable chemical potential. The real crystal is electrically neutral and therefore only combinations of point defects are possible, which balance to ensure that the total charge is zero. This is embodied in the so-called *charge neutrality* condition. In common usage, there is a further assumption implicit in the charge neutrality condition: at least a pair, and sometimes more, of the charged defects are far more abundant than all other defects, and balancing the charges on these amounts to ensuring

neutrality of the overall crystal. The defects appearing in the charge neutrality condition are consequently called the *majority defects*, and each neutral combination of these is called a *disorder type*. See Schmalzried (1983) for details on these and other related definitions used in this work.

In defining the chemical potential of a structural unit $\alpha$, an activity coefficient, $a_\alpha$, is introduced using the conventional formalism:

$$\mu_\alpha = \mu_\alpha^0 + RT\ln(a_\alpha), \tag{1}$$

where $\mu_\alpha^0$ is the chemical potential of $\alpha$ in the chosen reference state—often taken to be the perfect single crystal. In this commonly chosen reference state the crystallographic sites are fully occupied by regular structural units, without any point defects. In the present case where we consider a solid solution of fayalite and forsterite and focus on incorporation of defects such as vacancies into these, we have two options: (1) we could either define a different reference state for each olivine with a different Fe/(Fe+Mg)-ratio and consider the incorporation of defects into each one of these separately, or (2) use one fixed reference state for the whole solid solution series (for example, that of perfect and pure fayalite). We have chosen pure fayalite as the reference state for all point defects and structural units in olivines of all compositions.

Since point defects in general are highly diluted constituents, it is typically assumed that the chemical potentials of the regular structural units is almost identical to that in the reference state. Note that this is only valid if the first option of a different reference state for each major element composition (Fe/Mg ratio in this case) is used, not for the choice we have made. For the dilute point defects it is assumed that they behave ideally i.e., $a_\alpha = [\alpha]$, or that they obey Henry's law, i.e., $a_\alpha = \gamma\,[\alpha]$, where $\gamma$ is a constant. First, this depends on the choice of standard states as well. Even for a choice of standard state of type (1), this holds only if there is no interaction with other point defects, which is justified if the point defects are randomly distributed within the crystal (e.g., there is no association of defects). For the choice of standard states that we have made, and some of the models we will be discussing, therefore, introduction of non-constant activity coefficients is unavoidable for the accurate description of chemical potential of point defects in olivines of different compositions. The simplified thermodynamic analysis in Appendix B shows that within the framework of a ternary simple mixture mixing model and subject to certain assumptions, the activity of point defects can be described by an equation of the form

$$RT\ln\left(\gamma_{V''_{Me}}(X_{Fe})\right) = W_{VMe} + \bar{W}\cdot X_{Fe} - \bar{W}\cdot (X_{Fe})^2, \tag{2}$$

where the simplified activity coefficient $\gamma_{V''_{Me}}$ can be expressed in terms of the fayalite content, $X_{Fe}$, and two averaged interaction parameters, $W_{VMe}$ and $\bar{W}$ (or, with further simplifying assumptions, only one parameter, $W_{VMe}$, see Appendix B).

Thus, we introduce for each point defect $\alpha$ an activity coefficient $\gamma_\alpha(X_{Fe})$, which is an explicit function of the fayalite content. For example, for the chemical potential of vacancies on the metal site of an olivine of a defined composition, one obtains

$$\begin{aligned}\mu_{V''_{Me}} &= \mu^0_{V''_{Me}} + RT\ln\left(a_{V''_{Me}}\right)\\ &= \mu^0_{V''_{Me}} + RT\ln\left(\gamma_{V''_{Me}}(X_{Fe})\cdot[V''_{Me}]\right);\end{aligned} \tag{3}$$

analogous expressions can be written for any other structural unit. Treatment of non-ideal behavior in the analysis is essential because point defect concentrations and experimentally determined ''equilibrium constants'' (see ''Critical evaluation of existing experimental data'' for clarification of the quotes) for the defect forming reactions in olivines at isothermal, isobaric conditions are strong functions of compositions, as will be seen below.

## Point defect models and related thermodynamics

There appears to be agreement in the literature that $V''_{Me}$ and $Fe^{\bullet}_{Me}$, equivalent to electron holes, are the most abundant point defects in olivine restricted completely to the $Fe^{2+}$–Mg binary join over a wide range of thermodynamic conditions. This inference is based on results of thermogravimetric measurements (Nakamura and Schmalzried 1983; Tsai and Dieckmann 2002), diffusion data (e.g., Nakamura and Schmalzried 1984; Chakraborty 1997; Petry et al. 2004), electrical conductivity data (Sato 1986; Wannamaker and Duba 1993, and Barkmann and Cemic 1996), and to some extent ab-initio calculations ($V''_{Me}$ in pure forsterite, Brodholt 1997). Additional defects suggested as being important are $V''''_{Si}$, $O^{\bullet\bullet}_i$ (Hirsch and Shankland 1991) and $Fe'_{Si}$ (Nakamura and Schmalzried 1983). Since Si and O diffusion in olivine is many orders of magnitude slower than diffusion of ions occupying the metal site (Dohmen et al. 2002 and Petry et al. 2004), oxygen vacancies and silicon interstitials are unlikely candidates for majority defects.

In the standard point defect model developed by Nakamura and Schmalzried (1983) on the basis of thermogravimetric measurements with synthetic olivine, $V''_{Me}$ is charge compensated by $Fe^{\bullet}_{Me}$. To explain their observations completely they had to postulate that some of the $Fe^{3+}$ occupy the Si site and these dects are strongly associated with $Fe^{3+}$ on the metal site, $Fe^{\bullet}_{Me}\,Fe'_{Si}$, to form a

neutral defect complex. In the more recent model of Tsai and Dieckmann (2002) the association is not necessary to explain their thermogravimetric data. The effective charge balance condition in this case would be:

$$2[V''_{Me}] + [Fe'_{Si}] = [Fe^{\bullet}_{Me}], \tag{4a}$$

For a complete association, or if the concentration of $Fe^{3+}$ on the Si site is negligible, the final charge neutrality condition is reduced to:

$$2[V''_{Me}] = [Fe^{\bullet}_{Me}]. \tag{4b}$$

In general, to define the point defect chemistry of a four component (e.g., Fe, Mg, Si and O) non-stoichiometric olivine, it is necessary to define three variables (e.g., $a(SiO_2)$, $fO_2$ and $a(Fe_2SiO_4)$ in addition to pressure ($P$) and temperature ($T$), i.e., $n$–1 variables need to be fixed, where $n$ is the total number of independent chemical components to completely define the state of a phase at constant $P$ and $T$. Following NS83 and TD02, two alternatives are considered below for defining the point defect chemistry at a given $P$, $T$, $X_{Fe}$ and $fO_2$: either $a(SiO_2)$ or the cationic ratio $\xi$ = [Si]/([Si]+[Fe]+[Mg]) is constrained. The former corresponds to a situation where an olivine behaves as an open system and an external agent can impose an $a(SiO_2)$, the latter corresponds to a closed system behavior, e.g., in an experiment at lower temperatures simply because exchange of cations with the environment is kinetically hindered. The thermodynamic description of these two situations is different, which needs to be considered in order to analyze the data covering a wide range in temperature.

For the first case of fixed $a(SiO_2)$, the following reactions can be formulated for the formation of the majority point defects in olivine:

$$6 \cdot Fe^{x}_{Me} + SiO_2 + O_2(g) = 2 \cdot V''_{Me} + 4 \cdot Fe^{\bullet}_{Me} + Fe_2SiO_4, \tag{5a}$$

$$Fe^{x}_{Me} + Si^{x}_{Si} + 1/2O_2(g) + 1/2Fe_2SiO_4 = Fe^{\bullet}_{Me} + Fe'_{Si} + 3/2SiO_2 \tag{5b}$$

Reaction 5a is a net transfer reaction where metal vacancies are formed by oxidation of $Fe^{2+}$ on octahedral sites to $Fe^{3+}$, coupled with the formation of a new formula unit of fayalite on the surface by transfer of $SiO_2$ (e.g., from orthopyroxene or a melt) and gaseous $O_2$ from an external source. The corresponding mass action laws for reactions 5a and b are:

$$K_{5a} = \exp\left(-\frac{\Delta G^0_{5a}}{RT}\right) = \frac{a_{Fe_2SiO_4}\left(a_{V''_{Me}}\right)^2\left(a_{Fe^{\bullet}_{Me}}\right)^4}{\left(a_{Fe^{x}_{Me}}\right)^6 a_{SiO_2} f_{O_2}} \tag{6a}$$

$$K_{5b} = \exp\left(-\frac{\Delta G^0_{5b}}{RT}\right) = \frac{a_{Fe^{\bullet}_{Me}} a_{Fe'_{Si}} (a_{SiO_2})^{3/2}}{a_{Fe^{x}_{Me}} \cdot a_{Si^{x}_{Si}} (f_{O_2})^{1/2} (a_{Fe_2SiO_4})^{1/2}} \tag{6b}$$

Relating the activities to concentrations using expressions like (2) and (3), the final equations connecting point defect concentrations to thermodynamic parameters are as follows:

$$\log\left(K_{x(5a)}\right) = \log\left(K_{5a}/K_{\gamma(5a)}\right) = \log\left(\left[V''_{Me}\right]^2\left[Fe^{\bullet}_{Me}\right]^4\right) - 4\log\left(X_{Fe}\right) - \log\left(a_{SiO_2}\right) - \log\left(f_{O_2}\right) \tag{7a}$$

$$\log\left(K_{x(5b)}\right) = \log\left(K_{5b}/K_{\gamma(5b)}\right) = \log\left(\left[Fe'_{Si}\right]\left[Fe^{\bullet}_{Me}\right]\right) - \log\left(X_{Fe}\right) + 3/2\log\left(a_{SiO_2}\right) - 1/2\log\left(f_{O_2}\right) \tag{7b}$$

The explicit expression for $K_{\gamma(5a)}$, subject to certain assumptions, have been provided in Appendix B. Once $K_{x(5a)}$ and $K_{x(5b)}$ are known as explicit functions of the fayalite content (e.g., from experiments of NS83 and TD02), the equilibrium concentrations of $V''_{Me}$, $Fe^{\bullet}_{Me}$ and $Fe'_{Si}$ are the only unknowns and by solving Eq. 7a, b, and the charge neutrality condition (Eq. 4a) simultaneously, these equilibrium concentrations can be calculated as functions of $X_{Fe}$, $a(SiO_2)$ and $fO_2$. For a complete association of $Fe^{\bullet}_{Me}$ and $Fe'_{Si}$, or absence of $Fe'_{Si}$, just Eqs. 7a and 4b have to be solved simultaneously. Note also that replacing $[Fe^{\bullet}_{Me}]$ in Eq. 7a using the charge neutrality condition (4b), one obtains a stoichiometric coefficient of 6 for $[V''_{Me}]$, a fact that we make repeated use of later.

For the second case, where the cationic ratios are fixed, only one reaction is necessary to define the relevant point defect concentrations because the stoichiometric variable $\xi$ = [Si]/([Si] + [Fe] + [Mg]) is directly related to defects (Nakamura and Schmalzried, 1983):

$$\xi = \frac{1 - [Fe'_{Si}]}{3 - [V''_{Me}]} \tag{8}$$

This relationship, combined with the charge neutrality condition (Eq. 4a or 4b) leaves only one undetermined point defect concentration. To obtain this, a relevant reaction can be derived from reactions 5a and 5b, by multiplying reaction 5a by 3/2 and adding reaction 5b:

$$10Fe^{x}_{Me} + Si^{x}_{Si} + 2O_2(g) = 3V''_{Me} + 7Fe^{\bullet}_{Me} + Fe'_{Si} + Fe_2SiO_4 \tag{9}$$

The corresponding equilibrium constant is given by:

$$K_9 = K_{5a}^{3/2} \cdot K_{5b} = \frac{\left(a_{V''_{Me}}\right)^3 \cdot \left(a_{Fe^{\bullet}_{Me}}\right)^7 \cdot a_{Fe'_{Si}} \cdot a_{Fe_2SiO_4}}{\left(a_{Fe^{x}_{Me}}\right)^{10} \cdot a_{Si^{x}_{Si}} \cdot \left(f_{O_2}\right)^2} \tag{10}$$

and using again the activity–composition relations from above, it follows:

$$\begin{aligned} \log\left(K_{x(9)}\right) &= \log\left(K_9/K_{\gamma(9)}\right) \\ &= \log\left(\left[V''_{Me}\right]^3 \cdot \left[Fe^{\bullet}_{Me}\right]^7 \cdot \left[Fe'_{Si}\right]\right) \\ &\quad - 8\log\left(X_{Fe}\right) - 2\log\left(f_{O_2}\right) \end{aligned} \tag{11}$$

where $a_{si^{x}_{si}}$ has been assumed to be unity.

For a complete association of $Fe^{\bullet}_{Me}$ and $Fe'_{Si}$ Eqs. 9 and 11 are slightly modified to:

$$\begin{aligned} 10Fe^{x}_{Me} + Si^{x}_{Si} + 2O_2(g) = {} & 3V''_{Me} + 6Fe^{\bullet}_{Me} \\ & + \left\{Fe^{\bullet}_{Me}Fe'_{Si}\right\} + Fe_2SiO_4 \end{aligned} \tag{12}$$

$$\begin{aligned} \log\left(K_{x(12)}\right) &= \log\left(\left[V''_{Me}\right]^3 \cdot \left[Fe^{\bullet}_{Me}\right]^6 \cdot \left[\left\{Fe^{\bullet}_{Me}Fe'_{Si}\right\}\right]\right) \\ &\quad - 8\log\left(X_{Fe}\right) - 2\log\left(f_{O_2}\right) \end{aligned} \tag{13}$$

Knowing $K_{x(9)}$ enables one to calculate the point defect concentrations from Eqs. 4a, 8 and 11 (or alternatively from Eqs. 4b, 8 and 13 with $K_{x(12)}$) as a function of $\xi$ and $fO_2$.

## Point defect concentrations in pure (Fe,Mg)-olivine

### *Critical evaluation of existing experimental data*

From thermogravimetric measurements absolute values of $K_{x(12)}$ (e.g., Nakamura and Schmalzried 1983) or $K_{x(9)}$ (e.g., Tsai and Dieckmann 2002) can be determined. An alternate interpretation of the same data (open vs. closed system) allows $K_{x(5a)}$ and $K_{x(5b)}$ (e.g., Tsai and Dieckmann 2002) to be determined simultaneously. These reaction constants have been determined as a function of olivine composition in these two studies and in both cases the constants $K_x$ depend strongly on the fayalite content. Adequate description of this behavior requires incorporation of non-ideality in the formalism of the thermodynamic analysis, for which we have provided the simplest possible form in Appendix B. Neither NS83 nor TD02 have discussed this aspect in detail, although NS83 mention the possibility. In this context we want to note here that in both studies $K_x$ and not the equilibrium constants $K$ of the relevant reactions were determined, although the authors discuss their results in terms of determination of the equilibrium constant, $K$, in both works (explicitly in TD02 and implicitly, through the equation stated, in NS83). To deal with this problem in terminology, we will use ''equilibrium constant'' to refer to the usage by these authors, alerting the reader to the fact that a true equilibrium constant cannot be a function of composition and the quantity concerned is actually $K_x$ as defined in this work.

The main difference between the two experimental studies is that they used different containers for olivine. Tsai and Dieckmann (2002) criticized the data of Nakamura and Schmalzried (1983) because they used Pt-containers which are known to dissolve Fe in considerable amounts. Therefore an additional mass loss to the Pt-container may have occurred during their experiments, thereby introducing a systematic error to their data. Tsai and Dieckmann (2002) used quartz as a container material for olivine and discussed the possibility of buffering the activity of $SiO_2$ by the container. For Mg-rich olivine the formation of orthopyroxene is also likely, which would define the $SiO_2$ activity but might entail decomposition reactions of olivine as well. Thus, Tsai and Dieckmann (2002) considered various possible scenarios to analyze their data—either $\xi$ or $a(SiO_2)$ fixed (but the authors favored the former case), without any association of $Fe^{\bullet}_{Me}$ and $Fe'_{Si}$ in each case. In terms of the discussion detailed earlier, they have determined $K_{x(9)}$ or, alternately, $K_{x(5a)}$ and $K_{x(5b)}$.

Nakamura and Schmalzried (1983) used Eqs. 4b, 8 and 13 to analyze their data and determined the following fit for the constant $K_{x(12)}$ as a function of composition:

$$1,000 - 1,130\,^{\circ}\mathrm{C}: \quad \log K_{x(12)} = -22.197 + 14.70X_{Fe} - 8\log(X_{Fe}) \tag{14a}$$

$$1,200\,^{\circ}\mathrm{C}: \quad \log K_{x(12)} = -22.564 + 17.78X_{Fe} - 8\log(X_{Fe}) \tag{14b}$$

Note that $\log(K_{x(12)})$ of Nakamura and Schmalzried (1983) has been corrected here by a constant offset of 9 log(2) (where the 9 comes from the 3 $Fe^{3+}$ and 6 vacancies on the metal site) because they used site fractions instead of concentrations per formula unit in the mass action law.

Tsai and Dieckmann (2002) reported data at two temperatures, 1,130 and 1,200 °C. In Fig. 1a–c the $K_x$ as a function of fayalite content at 1,130 and 1,200 °C from the two studies are shown for comparison. As an additional constraint that can help evaluate consistency between the two thermogravimetric studies, we have calculated the values of $K_{x(9)}$ from the values of $K_{x(5a)}$ and $K_{x(5b)}$ of Tsai and Dieckmann (2002). The two experimental studies are contradictory in the sense that Nakamura and Schmalzried (1983) observed increasing values for $K_{x(12)}$ with temperature, while Tsai and Dieckmann (2002) observed a

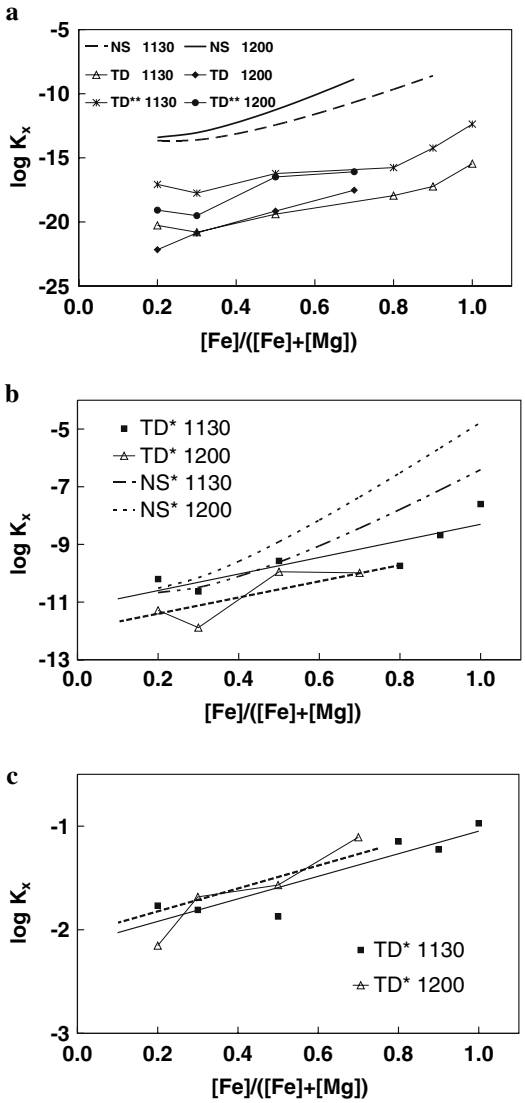


**Fig. 1** Experimental data for $K_{x(12)}$, $K_{x(9)}$ (**a**), $K_{x(5a)}$(**b**) and $K_{x(5b)}$ (**c**) of Nakamura and Schmalzried (1983) and Tsai and Dieckmann (2002) as a function of olivine composition at 1,130 and 1,200 °C. In the legend of the plots the different data are referred by symbols NS, NS*, TD, TD* and TD** which relate to different modes of analyzing the data by Nakamura and Schmalzried (NS) or Tsai and Dieckmann (TD). The conditions corresponding to individual symbols are defined in Table 1. In **b** and **c** the *solid line* represents a linear fit to the data of TD* at 1,130 °C. The *dashed line* is parallel to this fit and was chosen so as to represent the data of TD* at 1,200 °C

negative correlation of $K_{x(9)}$ with temperature (recall that Eq. 9 is simply the non-associated defect equivalent of 12) for forsterite-rich olivine. It is apparent that the constant $K_{x(9)}$ of Tsai and Dieckmann (2002) shows a different compositional dependence at 1,130 °C from that at 1,200 °C, so that the enthalpy change of the reaction (= temperature dependence) is negative for forsterite-rich compositions and positive for forsterite-poor compositions. This implies a highly unusual non-ideal thermodynamic behavior of the participants in this reaction—as the thermodynamic properties of most other participants are relatively well known, the unusual behavior, if real, must stem from unusual energetics of the point defects involved in the reaction. Indeed, as is seen clearly from the distance between the curves representing the same reaction at different temperatures in Fig. 1a (NS83 provide only the equation of their best fit line, lines connecting the data points of TD02 have been drawn here), the temperature dependence of each reaction is different for each olivine composition. This is unexpected for a temperature range of only 70 °C (e.g., see also the simplified thermodynamic model in Appendix B)—one would expect the curves for any reaction at different temperatures to be offset more or less parallel to each other. In general, NS83 find a weaker temperature dependence of $K_{x(12)}$. In fact, for the most forsterite-rich compositions they find no dependence at all, implying that the enthalpy change of this reaction is zero to negligible at these compositions. The temperature dependence of $K_{x(12)}$ does show (Fig. 1b) the expected regular behavior for the NS83 model but for TD02 one finds the crossover in temperature dependence across the compositional range once again (e.g., Fig. 1c); the expected behavior is shown in this case as a dotted line. Therefore, we can conclude that there is considerable uncertainty in the behavior of these models as a function of temperature and each data set has its own shortcomings. These need to be considered when we analyze diffusion data in terms of point defect chemistry and therefore we have considered various possible scenarios permitted by all the data, rather than prefer any one data set a priori. However, irrespective of the models, it is worth noting here already that any calculated defect concentration will be an upper limit because all possible systematic errors discussed above would lead to an overestimation of weight change and consequently, vacancy concentrations.

### *Calculation of the role of composition, oxygen fugacity and the use of different models and assumptions*

We have calculated the concentration of the majority point defects (cation vacancies, $V''_{Me}$, $Fe^{3+}$ in olivine, $Fe^{\bullet}_{Me}$, and $Fe^{3+}$ on Si sites, $Fe'_{Si}$) as a function of composition, temperature and oxygen fugacity by solving different combinations of the equations outlined above. The chosen conditions, point defect model (NS83 or TD02) and relevant combination of equations have been summarized in Table 1. For instance, by combining Eqs. 4b, 8, and 13 for an olivine with an ideal cationic ratio $\xi = 1/3$ the final equation for the metal vacancies is:

**Table 1** Point defect models, equations and data used for the calculation of point defect concentrations in pure and natural olivine

| Case | Majority point defects | Equations | Constraint | Thermodynamic data |
|---|---|---|---|---|
| 1 NS | $V''_{Me}$, $Fe^{\bullet}_{Me}$, $\{Fe^{\bullet}_{Me}\ Fe'_{Si}\}$ | 4b, 8, 13 | $\xi = 1/3$ | $K_{x(12)}$ (Eq. 14a, b, Fig. 1a)[a] |
| 2 TD | $V''_{Me}$ , $Fe^{\bullet}_{Me}$ , $Fe'_{Si}$ | 4a, 8, 11 | $\xi = 1/3$ | $K_{x(9)}$ (Fig. 1a)[b] |
| 3 TD* | $V''_{Me}$ , $Fe^{\bullet}_{Me}$ , $Fe'_{Si}$ | 4a, 7a, 7b | ol/opx[c] | (Fig. 2b–c) $K_{x(5a)} = (K'')^2 \cdot 1/4 \cdot (X_{Fe})^{-4} \cdot a^{-1}_{SiO_2}$ [d] $K'_{x(5b)} = K' \cdot (X_{Fe})^{-2} \cdot a^{3/2}_{SiO_2}$ |
| 4 TD** | $V''_{Me}$ , $Fe^{\bullet}_{Me}$ , $Fe'_{Si}$ | 4a, 8, 11 | $\xi = 1/3$ | $K_{x(9)} = K^{3/2}_{x(5a)} \cdot K_{x(5b)}$ (Fig. 1a)[d] |
| 5 NS-T | $V''_{Me}$ , $Fe^{\bullet}_{Me}$ , $\{Fe^{\bullet}_{Me}\ Fe'_{Si}\}$ | 4b, 7a, 8 | ol/opx[c] | For $X_{Fe} = 0.1$: Eq. 16[e] |
| 6 TD-T | $V''_{Me}$ , $Fe^{\bullet}_{Me}$,$Fe'_{Si}$ | 4a, 7a, 7b | ol/opx[c] | For $X_{Fe} = 0.1$:Eqs. 17a and b[f] |
| 7 NS-Ip | $V''_{Me}$, $Fe^{\bullet}_{Me}$,$\{Fe^{\bullet}_{Me}\}$,$IP^{\bullet}_{Me}$ | 7a, 8, 21b | ol/opx[c] | As case 5 NS-T[e] |
| 8 TD-Ip | $V''_{Me}$ , $Fe^{\bullet}_{Me}$ , $Fe'_{Si}$ , $IP^{\bullet}_{Me}$ | 7a, 7b, 21a | ol/opx[c] | As case 6 TD-T[f] |

All calculations were performed at $P = 10^5$ Pa and given $T$, $fO_2$, and $X_{Fe}$. The last thermodynamic constraint is given in the table

[a] $K_{x(12)}$ equivalent to $K_{19}$ of Nakamura and Schmalzried (1983)

[b] $K_{x(9)} = K_2$ of Tsai and Dieckmann (2002)

[c] $a(SiO_2)$ fixed by coexistence of ol and opx; for $X_{Fe} > 0.7$ $a(SiO_2) = 1$, since opx becomes unstable

[d] $K'$ and $K''$ of Tsai and Dieckmann (2002)

[e] Extrapolation of $K_{x(5a)}$ calculated from $[V''_{Me}]$ measured by Nakamura and Schmalzried (1983) at 1,130 and 1,200 °C for $X_{Fe} = 0.2$, for more details see text

[f] Extrapolation (to lower T and $X_{Fe}$) of $K'$ and $K''$ of Tsai and Dieckmann (2002)

$$\log\left(\left[V''_{Me}\right]\right) = \frac{1}{10}\log\left(K_{x(12)}\right) + \frac{8}{10}\log\left(X_{Fe}\right) + \frac{1}{5}\log\left(f_{O_2}\right) + \frac{1}{10}\log(3) - \frac{6}{10}\log(2) \quad (15)$$

For a given composition of olivine, this is an explicit function of $fO_2$, whereas the dependence on temperature ($T$) comes through the dependence of $K_{x(12)}$ on $T$ (e.g., Eq. 14). In other cases the relevant sets of equations (Table 1) have to be solved numerically. In Fig. 2a–c we illustrate the results of a few such calculations at different conditions and using different models. Figure 2a shows calculated vacancy concentrations on the metal site at different experimental temperatures and using different models for the entire olivine solid solution series. The total variation of the calculated vacancy concentration using various models and assumptions at any given $X_{Fe}$, $fO_2$ and temperature is within 0.4 log units (Fig. 2a). Oxygen fugacity has a larger effect on vacancy concentrations than variations due to the use of different models (e.g., compare Fig. 2b and Fig. 2c). The dependence is log-linear in all cases, with the only minor exception being case three in Table 1, which yields a slightly non-linear dependence of vacancy concentration on $\log fO_2$. The basic inference from all of these calculations is that in spite of all the uncertainties discussed above, the actual concentration of vacancies and other defects calculated using the various models, data and approximations at a given $X_{Fe}$ in the experimentally investigated temperature and $fO_2$ regime are well constrained.

*Calculation of the role of temperature*

Most relevant for an analysis of diffusion properties is, however, the temperature dependence of point defect concentrations and here the situation is very different, as we have already seen above. The first step is to extract temperature dependencies of the different point defect reactions from the experimental data that are free of internal inconsistencies such as those outlined above. One of the observations from Fig. 2a is that there is little difference in calculated vacancy concentrations if either $\xi$ or $a(SiO_2)$ is held constant (e.g., compare the models TD* and TD**, Table 1; Fig. 2a). Conversely, this implies that $\xi$ is close to the ideal value of 1/3 in the $SiO_2$ saturated cases at the experimental conditions. Therefore, assuming that the experiments of Nakamura and Schmalzried (1983) were almost $SiO_2$ saturated, one can use the calculated defect concentrations (e.g., case 1, Table 1) and a given $fO_2$ and olivine composition in Eq. 7a to calculate $K_{x(5a)}$. If this exercise is carried out at 1,130 and 1,200 °C, one obtains two values of $K_{x(5a)}$, which allow a temperature dependence to be calculated $\left(\ln\left(K_{x(5a),1,200}/K_{x(5a),1,130}\right) = -\Delta H/R(1/1,473 - 1/1,403)\right)$. However, as already noted, at some olivine compositions ($X_{Fe} = 0.1$ and $X_{Fe} = 0.2$) NS83 found no temperature dependence, neither did they observe any temperature dependence in experiments below 1,100 °C. Therefore, the evidence from their experiments is that the temperature dependence of this reaction is close to the resolution capabilities of their

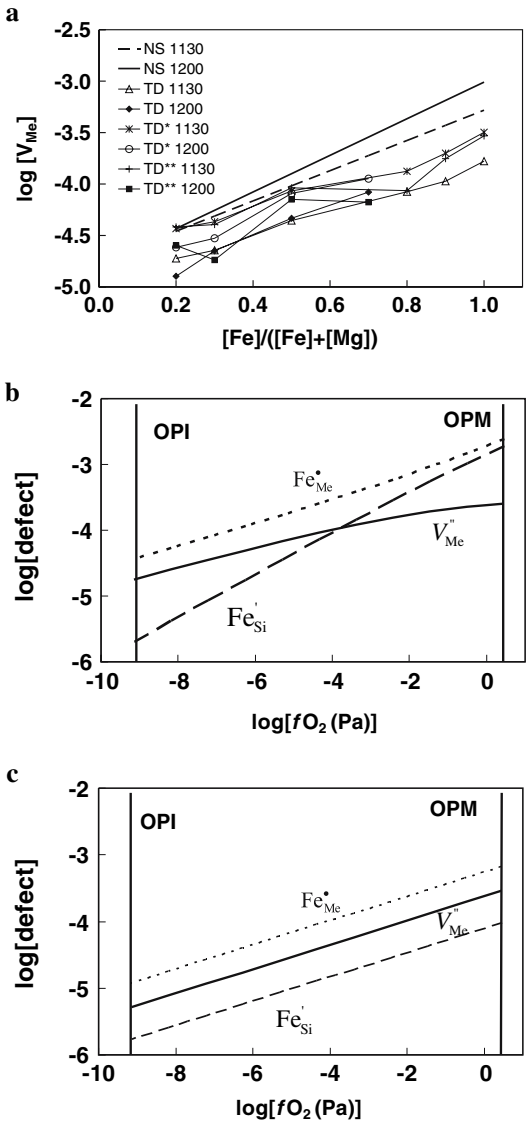


**Fig. 2** Concentrations of defects calculated for the different point defect models and data in comparison: (**a**) metal vacancies versus olivine composition at 1,130 and 1,200 °C at log($fO_2$, in Pa) = –7; majority defects as a function of log $fO_2$ at 1,130 °C for $X_{Fe}$ = 0.2 for the case 3 TD* (**b**) and case 1 NS (**c**). *Solid vertical lines* mark the upper and lower stability of olivine, see Appendix C for details

experiments; low in any case. We have used the maximum permissible temperature dependence allowed by the model of NS83 to obtain Eq. 16 for log $K_{x(5a)}$ below. We have used this value for all compositions in the calculations that follow. A similar exercise yields a very different picture for the dataset of TD02-independent of assumptions regarding constancy of $\xi$ or $a(SiO_2)$, one obtains a high and negative enthalpy change of the same reaction at an olivine composition of $X_{Fe}$ = 0.1. Therefore, in contrast to absolute concentrations and dependence on oxygen fugacity, the temperature dependency of vacancy concentrations calculated from the two models NS83 and TD02 are opposite extremes. Equations describing these contrasting temperature dependencies are:

$$\mathrm{NS83}: \log K_{x(5a)} = -7.32 - \frac{90\,\mathrm{kJ/mol}}{2.303RT}\left(\frac{1}{T}\right) \tag{16}$$

$$\mathrm{TD02}: \log K_{x(5a)} = -25.63 + \frac{396\,\mathrm{kJ/mol}}{2.303RT}\left(\frac{1}{T}\right) \tag{17a}$$

$$\log K_{x(5b)} = 3.217 - \frac{141\,\mathrm{kJ/mol}}{2.303RT}\left(\frac{1}{T}\right) \tag{17b}$$

The enthalpy change of the defect-forming reaction (5a) thus obtained (+90 or –396 kJ/mol) may be translated to the enthalpy of formation of a single vacancy by dividing by six, the stoichiometric coefficient for a vacancy in Eq. 5a (after incorporation of the charge neutrality condition 4b, as noted above). This yields the vacancy formation enthalpies, $\Delta H_f$, of 15 kJ/mol (a maximum, see above) for the NS83 model and –66 kJ/mol for the TD02 model.

At a given temperature Eqs. 16 or 17 (depending on choice of model) yield values of $K_{x(5a)}$ and $K_{x(5b)}$, which can be used with arbitrary values of $fO_2$ within the stability field of olivine and either Eqs. 4b and 7a (Table 1, case 5: NS-T) or Eqs. 7a, 7b and 4a (Table 1, case 3: TD-T) to solve simultaneously for the concentrations of the three majority defects $V''_{Me}$, $Fe^{\bullet}_{Me}$ and $Fe'_{Si}$(or $\{Fe'_{Si}\ Fe^{\bullet}_{Me}\}$). The resulting data can be fitted to an equation of the form

$$\log\left(\left[V''_{Me}\right]\right) = \log\left(\left[V''_{Me}\right]^{\circ}\right) + 1/n\log\left(fO_2/10^{-7}\right) - \frac{\Delta H_f}{2.303RT}, \tag{18}$$

where we have used a $fO_2$ of $10^{-7}$ Pa arbitrarily as reference $fO_2$. For metal vacancies in olivines with $X_{Fe}$ = 0.1 at temperatures below 1200 °C, the values of $\Delta H_f$ for $V''_{Me}$ are found to be 15 kJ/mol (NS83) and –66 kJ/mol (TD02), which have already been obtained through a simplified analysis above and therefore serve to underscore the internal consistency of the approach. Similar equations may be formulated for any other defect. The values for $\Delta H_f$ (temperature dependence), $n$ ($fO_2$ dependence), and log ($[V''_{Me}]^{\circ}$) for vacancies as well as for $Fe^{\bullet}_{Me}$ and $Fe'_{Si}$(or $\{Fe'_{Si}\ Fe^{\bullet}_{Me}\}$) at this olivine composition are summarized in Table 2, calculations for any other olivine composition may be carried out using the same procedure. The general behavior one observes is that: (1) concentrations of $V''_{Me}$ becomes larger with $X_{Fe}$, (2) the $fO_2$ stability field becomes smaller with the increase in $X_{Fe}$, and (3) the enthalpy change of reaction (12) changes slightly with the change in $X_{Fe}$.

In Fig. 3a and b the results of the calculations for $V''_{Me}$ are displayed for an olivine with $X_{Fe}$ = 0.1. The dotted

**Table 2** Dependencies of the three majority point defects on thermodynamic parameters for the models and data of NS-T and TD-T (Table 1)

| Model | TD-T | | | NS-T | | |
|---|---|---|---|---|---|---|
| Point defect | $\Delta H_f$ (kJ/mol) | $n$ | [defect]° | $\Delta H_f$ (kJ/mol) | $n$ | [defect]° |
| $V''_{Me}$ | –66 | 1/6 | –7.177 | 15 | 1/6 | –4.042 |
| $Fe^{\bullet}_{Me}$ | –66 | 1/6 | –6.839 | 15 | 1/6 | –3.741 |
| $Fe'_{Si}$ | 207 | 1/3 | 2.178 | | | |
| $\{Fe^{\bullet}_{Me}\ Fe'_{Si}\}$ | | | | 15 | 1/6 | |

The three parameters listed in each case are defined through Eq. (18)

lines represent calculations at constant $fO_2$, but for various temperatures. The solid lines represent calculations at variable $fO_2$ at either the upper (OPM) or lower (OPI) phase boundary in the $fO_2$-$T$ space (see Appendix C, $\log(fO_2)_{OPM}$, Eq. 39, and $\log(fO2)_{OPI}$, Eq. 38, respectively). The observed vacancy concentration as a function of temperature and $fO_2$ is a sum of two effects (e.g., Eq. 18) which may complement or compete against each other. The first influence is the direct effect of temperature (termed $\Delta H$-*effect* below), expressed through the sign and magnitude of enthalpy change of the defect-forming reaction (e.g., Eqs. 16, 17). This is low and positive (~90 kJ/mol) for the NS83 model, higher in magnitude and negative (~ –396 kJ/mol) for the TD02 model. The second effect is the influence of $fO_2$ (termed $fO_2$-*effect* below), which is more complicated. Because of the relatively large enthalpy changes of reactions 34 and 35 (555 and 509 kJ/mol, respectively) marking the stability of olivine, the $fO_2$ at which olivine is stable decreases drastically with temperature. This drop in $fO_2$ results in a large drop in vacancy concentration, as seen from empirical equations such as (15) and (18) or from an application of Le Chatelier's principle to chemical equations such as (5a), (9) or (12) directly. Therefore, there is a second, indirect but larger influence of temperature on vacancy concentrations through the dependence of $fO_2$ on temperature. This effect is the same and constant for all models, given by the stoichiometry of the defect- forming reactions (e.g., 5a,5b,9 or 12) and thermodynamic properties of phases that determine the stability of olivine.

The effect of temperature alone (the $\Delta H$-*effect*) is illustrated by the dotted lines at constant $fO_2$ in Fig. 3a and b and is responsible for the very different appearances of Fig. 3a and b. The change of metal vacancy concentrations along the stability limiting reactions of olivine (OPI and OPM) with decreasing temperature, shown as dashed lines in Fig. 3a and b, have been calculated using the $T$ - $fO_2$ conditions along the stability curves in the calculation scheme outlined at the beginning of this section or alternately, directly in Eq. (18). Having calculated the vacancy concentrations, it is easy to rationalize the observed slope of these lines in Fig. 3a and b. The effect of variation of $fO_2$ along any one of these lines can be obtained (~90 kJ/mol) by simply multiplying the enthalpy change of the stability limiting reaction (~500 kJ/mol) by the $fO_2$ exponent (1/6) of the defect forming reaction as a simple consequence of the mass action law applied to Eq. 34 and 35.

Therefore the total temperature dependence of vacancy concentrations along these lines is given by the sum of these two effects, an apparent enthalpy of vacancy formation along a stability curve, $\Delta H_f^{stab}$: 90 + 15 = 115 kJ/mol for the NS83 model and 90–66 = 27 kJ/mol for the TD02 model. This explains the somewhat anomalous observation that in the TD02 model shown in Fig. 3a, the slope of the solid lines are close to zero (the $\Delta H$-*effect* and $fO_2$-*effect* compete against each other) in spite of the

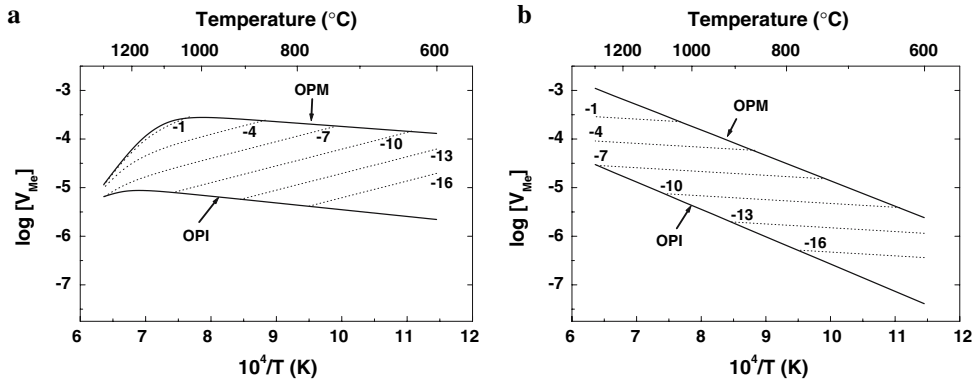


**Fig. 3** Concentration of metal vacancies within the stability field of olivine between 600 and 1,300 °C using **a** data of Tsai and Dieckmann (case 6, TD-T) and **b** data of Nakamura and Schmalzried (case 5, NS-T). The *dotted lines* are for a constant $fO_2$, the numbers on the curves indicate log ($fO_2$, in Pa). *Solid lines* are calculated for $fO_2$ (T) = OPM or OPI reactions (defined in Appendix C, Eq. 34 and 35, respectively) constraining the stability of olivine

high defect formation enthalpies; whereas in the NS83 model shown in Fig. 3b the slopes are steep, even though the defect formation enthalpies are close to zero. The dotted lines in contrast, showing only the $\Delta H$-*effect*, show a steep negative slope in Fig. 3a (TD02) and are practically horizontal on Fig. 3b (NS83), as expected.

The relatively high and negative enthalpy of defect formation in the TD02 model has some important consequences for extrapolations to higher and lower temperatures. At temperatures lower than 1,100 °C, the concentration of $Fe^{3+}$ on the Si site becomes negligible and the effective charge neutrality condition changes from Eq. 4a to 4b and therefore only reaction 5a becomes relevant for the formation of vacancies and $Fe^{3+}$. This is also evident from the Fig. 2b, because here it can be seen that at the more reducing conditions at 1,200 °C the concentration of $Fe^{3+}$ on the Si site is much smaller than the vacancy concentration. At lower temperatures, where the conditions are even more reducing, the concentration of $Fe^{3+}$ on the Si site is calculated to be even lower and its contribution to the charge neutrality condition can be completely neglected. As a further consequence, the logarithm of the concentration of metal vacancies is strictly proportional to 1/6 log $fO_2$, which can be derived by combining Eqs. 4b and 7a (unlike the situation above 1,200 °C).

At higher temperatures a third effect occurs in the TD02 model (e.g., case 3 (TD*)). $Fe^{3+}$ partitions increasingly into the Si site and consequently, when Fe in olivine is oxidized it disproportionates between the metal and the silicon site. With an increase of this effect with temperature, the concentration of metal vacancies required to compensate for $Fe^{3+}$ decreases and ultimately becomes independent of $fO_2$. This can be thought of as a saturation of the metal site with $Fe^{3+}$. This explains the change in slope and ultimately collapse of all lines to a point at high temperatures in Fig. 3a. However, formation of purely intrinsic metal vacancies by the formation of Frenkel defects (e.g., $Mg^{x}_{Me} = Mg^{\bullet\bullet}_{i} + V''_{Me}$) probably plays a larger role at higher temperatures and should be considered in addition. Since we do not have any data for this reaction and we want to focus in this work on the point defect chemistry of olivine at lower temperatures, this problem can be the topic of future studies.

## Effect of impurities on the point defect chemistry of olivine

Trace elements in natural olivine that can have concentrations within the concentration range of the majority point defects calculated above are Ni, Ca, Mn, Al, Cr, Ti, H, P and occasionally Na and V. Of these Ni, Ca and Mn are divalent cations that simply exchange with Fe and Mg, Ti exchanges with Si leaving the aliovalent ions $Al^{3+}$, $Cr^{3+}$, $P^{5+}$ and $H^{+}$ as likely candidates for incorporation as charged defect into the olivine structure. For instance, concentrations of Cr in San Carlos olivine (Part-I) are in the 100 ppm (by weight) range, which would be on the order of the $Fe^{3+}$ concentrations in pure olivine as calculated before. However, measuring concentration alone is not sufficient; the site occupancy of these ions is equally relevant. For example, the tri-valent ions could in part charge compensate themselves if the majority of $Al^{3+}$ occupied a Si site and $Cr^{3+}$ mainly a metal site. The situation could be expressed in Kroeger–Vink notation as $[Al'_{Si}] = [Cr^{\bullet}_{Me}]$ (e.g., as observed in orthopyroxene, Stalder et al. 2005). Therefore, exact concentrations of $Cr^{3+}$ and $Al^{3+}$ and the partitioning of $Al^{3+}$ between the Si and the metal site determine if the majority impurity defect is positively or negatively charged. Clearly, as already mentioned by Tsai and Dieckmann (2002), such roles of impurities have to be considered for a realistic charge neutrality condition, especially at lower temperatures where the vacancy concentrations in pure (Fe,Mg)-olivine calculated in ''*Calculation of the role of temperature*'' drop to low values. A complete charge neutrality condition for natural olivine would be:

$$2 \cdot [V''_{Me}] + [Fe'_{Si}] + [Al'_{Si}] = [Fe^{\bullet}_{Me}] + [Cr^{\bullet}_{Me}] + [Al^{\bullet}_{Me}] + [OH^{\bullet}_{O}] \quad (19)$$

Here we are mainly concerned with understanding point defect chemistry and diffusion mechanisms at low pressures and so we ignore the effect of H because only at pressures in the GPa range can significant concentrations of H of around 100 ppm be obtained in olivine (e.g., Bai and Kohlstedt 1993). Analysis of the effect of H could be the topic of a separate analysis.

In view of the potential complexities in the mode of occurrence of trivalent cations outlined above, we define an effective concentration of the trivalent impurities as the excess of $Al^{3+}$ and $Cr^{3+}$ on the metal site compared to $Al^{3+}$ on the Si site:

$$[IP3^{\bullet}_{Me}] = [Cr^{\bullet}_{Me}] + [Al^{\bullet}_{Me}] - [Al'_{Si}] \quad (20)$$

The charge neutrality condition Eqs. 4a or 4b are now replaced by:

$$2 \cdot [V''_{Me}] + [Fe'_{Si}] = [Fe^{\bullet}_{Me}] + [IP3^{\bullet}_{Me}] \quad (21a)$$

$$2 \cdot [V''_{Me}] = [Fe^{\bullet}_{Me}] + [IP3^{\bullet}_{Me}] \quad (21b)$$

With this change we have calculated the point defect chemistry of natural olivine within its stability field with the two different models and thermodynamic data available

for the majority defects (case 7 and case 8, Table 1) following procedures completely analogous to those for pure (Fe,Mg)-olivine described in detail earlier. The main assumption in these calculations is that the effective concentration of the trivalent impurities, $[IP3^{\bullet}_{Me}]$ is positive and constant, which means it is independent of $fO_2$ as well as temperature. The calculations were performed for four different values of $[IP3^{\bullet}_{Me}]$: 5 ppm (NS83), 20 ppm (TD02), 10 ppm (both) and 100 ppm (both) all in atomic formula units at constant $a(SiO_2)$ defined by coexistence of ol/opx for $Fo_{90}$ olivine. The results are illustrated in the same kind of figures as for pure olivine (Fig. 4a–d). It shows that with decreasing temperature the concentration of $V''_{Me}$ becomes less $fO_2$ dependent until below a critical temperature and $fO_2$ it becomes almost constant. The value of this critical temperature depends, of course, on the concentration of the impurity and becomes larger with increasing impurity levels. On the other hand, the impurities have a different effect on the concentration of $Fe^{\bullet}_{Me}$ than on that of $V''_{Me}$. The $fO_2$ dependence of the concentration of $Fe^{\bullet}_{Me}$ becomes even stronger than for pure olivine (not shown). It changes progressively from an exponent of 1/6 to an exponent of 1/4. This can be derived again from the mass action law of Reaction 5a (Eq. 7a) if the value of $[V''_{Me}]$ is set to a constant value (as is the case in the PED regime). As a net effect the concentration of $Fe^{3+}$ in natural olivine is smaller than in pure olivine.

Qualitatively this kind of behavior is observed for both data sets, but the effect of the impurities in case 7 (NS-Ip) is much more pronounced and starts to become significant at higher temperatures compared to case 8 (TD-Ip). However, because of the negative formation enthalpy in case 8 (TD-Ip) at constant oxygen fugacity one observes a counterintuitive behavior that at higher temperatures the disorder is pure extrinsic and at lower temperatures it is more transition metal extrinsic (see for example the line for an $fO_2$ of $10^{-13}$ Pa in Fig. 4b). But this effect of the formation enthalpy is overcome by the effect of the enthalpy change of the reactions OPI and OPM so that as a net effect again with decreasing temperature the concentration range of vacancies decreases.

Another effect of the impurities is that the apparent formation enthalpy, $\Delta H_a$, of the metal vacancies (the enthalpy obtained by fitting the log concentration of the metal vacancies by Eq. 18) depends on the $fO_2$ and becomes smaller with increasing impurity concentration. For instance at 100 ppm of $[IP3^{\bullet}_{Me}]$ and an $fO_2$ of $10^{-7}$ Pa the value of $\Delta H_a$ decreases from 15 to only 4 kJ/mol and from –66 to –37 kJ/mol for the NS83 and TD02 models, respectively.

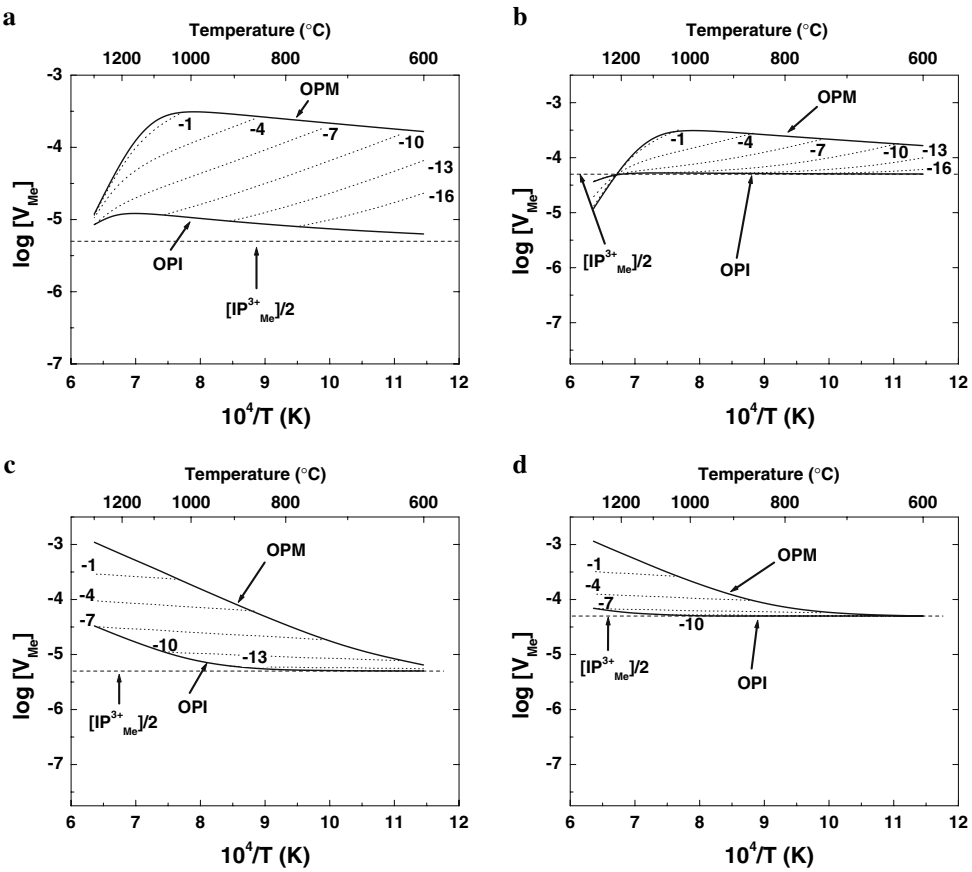


**Fig. 4** Concentration of metal vacancies within the stability field of olivine between 600 and 1,300 °C considering different impurity levels of a trivalent ion on the metal site (IP3) using data of Tsai and Dieckmann (case 8, TD-IP) **a** 10 ppm **b** 100 ppm, or data of Nakamura and Schmalzried (case 7, NS-IP) **c** 10 ppm **d** 100 ppm. The *dotted lines* are for a constant $fO_2$, the numbers on the curves indicate log ($fO_2$, in Pa). *Solid lines* are calculated for $fO_2$ ($T$) = OPM or OPI reactions constraining stability of olivine. The *thin dashed horizontal lines* represent the equivalent positive charge of the impurities on the metal site and is the lower limit for the concentration of metal vacancies in crystals containing the specified amounts of these trivalent ions. The only exception is at higher temperatures for case 8 (**b**), if the concentration of the $Fe^{3+}$ on the Si site becomes significant

The major consequence of these calculations is that kinetic processes controlled by concentration and mobility of the metal vacancies would become independent of $fO_2$ below a critical temperature and/or oxygen fugacity, as is observed for Fe–Mg diffusion in olivine below about $10^{-10}$ Pa (Part-I). This corresponds to a transition from a transition metal extrinsic (TaMED) mechanism to a pure impurity extrinsic (PED) mechanism as predicted by Chakraborty (1997); Part I and this work constitute the first experimental demonstration of this effect in any material. The exact condition at which change of the disorder type in the crystal from TaMED to PED occurs is a function of $T$ and $fO_2$ and depends on the value of $[IP3^{\bullet}_{Me}]$. In the PED regime (low $T$ or $fO_2$) the concentration of vacancies is larger compared to what would be found in pure olivine at comparable conditions (e.g., compare Figs. 3 and 4). Hence diffusion coefficients in natural olivine are expected to be slightly larger than in pure olivine at comparable conditions. Note however that the effect on apparent activation energies as inferred from an Arrhenius plot may be counter intuitive; we discuss this aspect in detail after deriving a quantitative relation between the concentration of $V''_{Me}$ and $D_{FeMg}$ to link the calculations of this paper with the experimental data presented in Part-I.

## Relation between point defects and diffusion: interpretation of experimental data on $D_{FeMg}$

### Theory

The basic assumption is that Fe and Mg diffuse via a vacancy mechanism. The self diffusion coefficient of Fe and Mg are then directly related to the concentration of the metal vacancies (e.g., see Dieckmann and Schmalzried, 1975), so that for Fe one has:

$$D^*_{Fe} = \Gamma_{Fe} \cdot f_{Fe} \cdot \lambda^2 \cdot \left[V''_{Me}\right] \tag{22}$$

where $D^*_{Fe}$ is the self diffusion coefficient at a given composition, $X_{Fe}$, and $f_{Fe}$ is the correlation factor for Fe, which itself depends on the jump frequency $\Gamma_{Fe}$ and $X_{Fe}$, and $\lambda$ is the jump distance to the nearest neighboring M site. The chemical diffusion coefficient for inter-diffusion of Fe and Mg, $D_{Fe-Mg}$ in olivine can be expressed in terms of their self diffusion coefficients (e.g., Barrer et al. 1963; Manning 1968; Lasaga 1979):

$$D_{(Fe-Mg)} = \frac{D^*_{Fe} \cdot D^*_{Mg}}{X_{Fe} \cdot D^*_{Fe} + X_{Mg} \cdot D^*_{Mg}} \Theta \tag{23}$$

Assuming the nearly ideal behavior of olivine solid solution (i.e., the thermodynamic factor, $\Theta \sim 1$) one obtains from Eq. 22 and the analogous equation for Mg:

$$D_{(Fe-Mg)} = \lambda^2 \cdot [V''_{Me}](aSiO_2, fO_2, X_{Fe}, T, P) \cdot \bar{\Gamma}_{FeMg}(T, P, X_{Fe}) \tag{24a}$$

where

$$\bar{\Gamma}_{FeMg}(T, P, X_{Fe}) := \frac{\Gamma_{Fe} \cdot f_{Fe} \cdot \Gamma_{Mg} \cdot f_{Mg}}{X_{Fe} \cdot \Gamma_{Fe} \cdot f_{Fe} + X_{Mg} \cdot \Gamma_{Mg} \cdot f_{Mg}} \tag{24b}$$

is defined to be an averaged jump frequency for inter-diffusion of Fe and Mg. $\bar{\Gamma}_{FeMg}$ depends for a given forsterite content only on temperature and pressure. We find that the diffusion coefficient for inter-diffusion of Fe and Mg is directly proportional to the site fraction of vacancies on the octahedral cation site. For the subsequent derivations, primarily designed to interpret the experimental data of paper I, we assume a constant pressure of 1 atmosphere. The temperature dependence of $\bar{\Gamma}_{FeMg}$ is assumed to follow an Arrhenian behavior, since the atomic jumps are thermally activated:

$$\bar{\Gamma}_{FeMg} := \bar{\Gamma}^{\bullet} \exp\left(\frac{-\Delta\bar{H}_m}{RT}\right) \tag{25}$$

where the activation energy, $\Delta\bar{H}_m$, is defined to be the averaged migration enthalpy. By inserting Eq. 25 and the empirical equation for the vacancy concentration of pure olivine (Eqs. 18 into 24a), the following equation is obtained for log $D_{FeMg}$ in pure (Fe,Mg)-olivine:

$$\log D_{FeMg} = \log(\lambda^2 \cdot \bar{\Gamma}^{\bullet} \cdot [V]^{\circ}) + \frac{1}{n}\log(fO_2/fO_2^{\circ}) - \frac{\Delta H_f + \Delta\bar{H}_m}{2.303RT} \tag{26}$$

Here, it is implicitly assumed that the point defects equilibrate almost instantaneously during the diffusion experiment, which is not unrealistic, as we have seen in Part I.

### Calculation of Fe–Mg diffusion coefficients within the complete stability field of natural olivine

The experimental data for Fe–Mg diffusion in olivine covers only a limited $fO_2$-$T$ range compared to the complete stability field, mainly because of the large experimental effort required to obtain each data point. We note in particular that with the technological advances outlined in Paper-I, kinetic hindrance is not a barrier any more down to temperatures of about 600 °C. However, the diffusion coefficients for the complete stability field can be reconstructed with Eqs. 24a or 26, if the point defect concentrations are known and diffusion data are available for a number of different temperatures and $fO_2$. Essentially, in

Eq. 26, for any given $T$ and $fO_2$, the terms $n$, $\Delta H_f$ and [V]° are known from the point defect models (e.g., Table 2) and the terms $\lambda^2 \cdot \bar{\Gamma}^\circ$ and $\Delta H_m$ need to be determined from the diffusion data. This approach is illustrated in the following, where the point defect concentrations for natural olivine are calculated with the models of both NS83 and TD02. In fact, this is a way to test if the diffusion data and the point defect data are consistent with each other, as will be seen below.

The first step in the calculation is to extract the value of the product $\lambda^2 \cdot \bar{\Gamma}_{FeMg}$. This value is calculated for a number of temperatures at a constant $fO_2$ (done here at $10^{-7}$ Pa, where we have the best experimental constraint) simply by taking the ratio of the measured $D_{FeMg}$ and the calculated $[V''_{Me}]$ (compare with Eq. 24a). The calculated logarithmic values of this product were then fitted by Eq. 25 (multiplied with $\lambda^2$) on an Arrhenius plot and the slopes and intercepts yield values for $\Delta \bar{H}_m$ and $\lambda^2 \cdot \bar{\Gamma}^\circ$ (Fig. 5). The value of the jump distance is assumed to be effectively temperature and pressure independent since the effects of thermal expansion and compressibility are minor compared to the thermal activation of the atomic jumps. For the given diffusion dataset, the calculated migration energy depends not only on the point defect model (the defect formation enthalpy within the TaMED regime, which is different from intrinsic defect formation energies) but in addition on the impurity concentration. Depending on the effective impurity concentration (10 or 100 ppm) the migration enthalpy varies between 186 and 194 kJ/mol for NS83 and 267 and 236 kJ/mol for the TD02 models, respectively. The reason for this is that the migration enthalpy, $\Delta H_m$, is equal to the difference between the activation energy of diffusion, $Q$ (= 201 kJ/mol at $fO_2$ = $10^{-7}$ Pa) and the apparent defect formation enthalpy of the vacancies, in this case at an $fO_2$ of $10^{-7}$ Pa, $\Delta H_f$ ( = 15 or –66 kJ/mol + a term which depends in turn on $[IP3^{\bullet}_{Me}]$), as shown above. Indeed, the migration energy of metal vacancies determined by Kohlstedt and Mackwell (1998), 260 kJ/mol, fits perfectly with the migration energy derived here from the point defect model TD02 using an impurity level of 20 ppm.

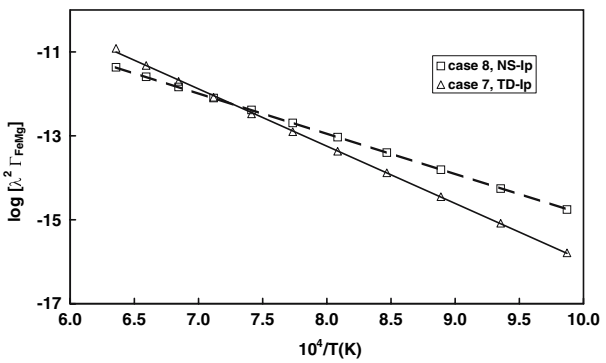


**Fig. 5** Arrhenius-plot of the product $\lambda^2 \cdot \bar{\Gamma}_{FeMg}$ as calculated from the combination of experimental diffusion data along [001] and point defect data for an effective trivalent impurity content on the metal position of 10 ppm a.f.u. for the cases TD-IP and NS-IP. *Straight lines* (*solid* and *dashed*) are linear fits, which were used to determine $\Delta \bar{H}_m$ and $\lambda^2 \cdot \bar{\Gamma}^\circ$. For the given impurity content, migration enthalpies of 186 kJ/mol (NS-IP model) and 267 kJ/mol (TD-IP model) are obtained, respectively

Knowing now $\Delta \bar{H}_m$ and $\lambda^2 \cdot \bar{\Gamma}^\circ$, Fe–Mg diffusion coefficients may be calculated using Eqs. 24a and 25 and the values for $[V''_{Me}]$ at any $fO_2$ and $T$ within the complete stability field of olivine. At this point we want to note that our experiments (Part-I) covered the more reducing end within the stability field of olivine. Thus, the effect of trivalent impurities is likely to be seen at temperatures around 1,000 °C, as long as the $[IP3^{\bullet}_{Me}]$ is positive and in the 10 to a few 100 ppm (a.f.u) range. For larger concentrations, effects could be seen already at about 1,100 °C depending on the enthalpy change of reaction 5a. In any case, a key observation is that the transition occurs over a wide range in temperature and $fO_2$ (e.g., several 100° and several decades in $fO_2$, see Fig. 6a–d), so that it is a smeared transition rather than a kink on an Arrhenius plot. As we shall see below, this makes it difficult to derive a general equation for calculating diffusion coefficients in olivine as a function of various intensive parameters.

The results of the calculations are illustrated in Fig. 6a–d again for both defect models (NS83* and TD02*) in comparison with the experimental data. Analogous to vacancy concentrations in Figs. 3 and 4, log $D_{FeMg}$ for various temperatures at a constant $fO_2$ are shown along with variation of $D_{FeMg}$ along the upper and lower boundaries of the stability field of olivine. Independent of the dataset used, it can be stated that in comparison to pure olivine the behavior of cation diffusion in natural olivine changes significantly (cf. Fig. 4), even if the impurity levels are relatively small (e.g., 5 ppm, NS83). The effect of the tri-valent impurities can be summarized in three points: (1) With decreasing temperature the range of $D_{FeMg}$ at a given temperature, due to variation in $fO_2$, decreases. This effect is more pronounced in the case of data NS83 and increases in general with increasing concentration of $[IP3^{\bullet}_{Me}]$ and increasing defect formation enthalpy. This is a consequence of the fact that at a given temperature below a critical oxygen fugacity the vacancy concentration in a pure (Fe,Mg)-olivine (due to presence of $Fe^{3+}$ only) is well below the impurity concentrations being considered here. (2) On the average, with decreasing temperature the dependence of $D_{FeMg}$ on $fO_2$ decreases and the log $D_{FeMg}$ may show a non-linear dependence on log $fO_2$. (3) Below a critical temperature the diffusion coefficient becomes completely independent of $fO_2$, which happens only in case of the data set NS-Ip in the experimentally investigated temperature range if the

effective impurity concentration is around 100 ppm (can be inferred from Fig. 4d and Eq. 24a).

The main difference in behavior according to the two point defect models (NS83 and TD02) for metal cation diffusion in olivine is seen in the behavior at constant $fO_2$. In the case of NS-Ip the observed activation energy of diffusion (i.e., slope of data on Arrhenius plot) does not change significantly with temperature, whereas in the case of TD-Ip the activation energy becomes *larger* with decreasing temperature and $fO_2$, because of the large negative formation enthalpy of the metal vacancies (–66 kJ/mol) (can be inferred from Fig. 4b and Eq. 24a).

From the comparison of the calculated data for $D_{FeMg}$ with the measured data at different $fO_2$ and temperatures it can now be tested, which, if any, of the point defect models and concentration of $IP3^{\bullet}_{Me}$ are consistent with the experimental diffusion data. The data at $fO_2 = 10^{-7}$ Pa were used to convert the calculated vacancy concentrations to diffusion coefficients. So, only the data measured at an $fO_2$ of $10^{-10}$ and $10^{-12}$ Pa are relevant for testing models. The two most important indicators for the consistency of the point defect data with the diffusion data are (1) the critical $fO_2$ at which diffusion becomes insensitive to the redox conditions and (2) the activation energy observed

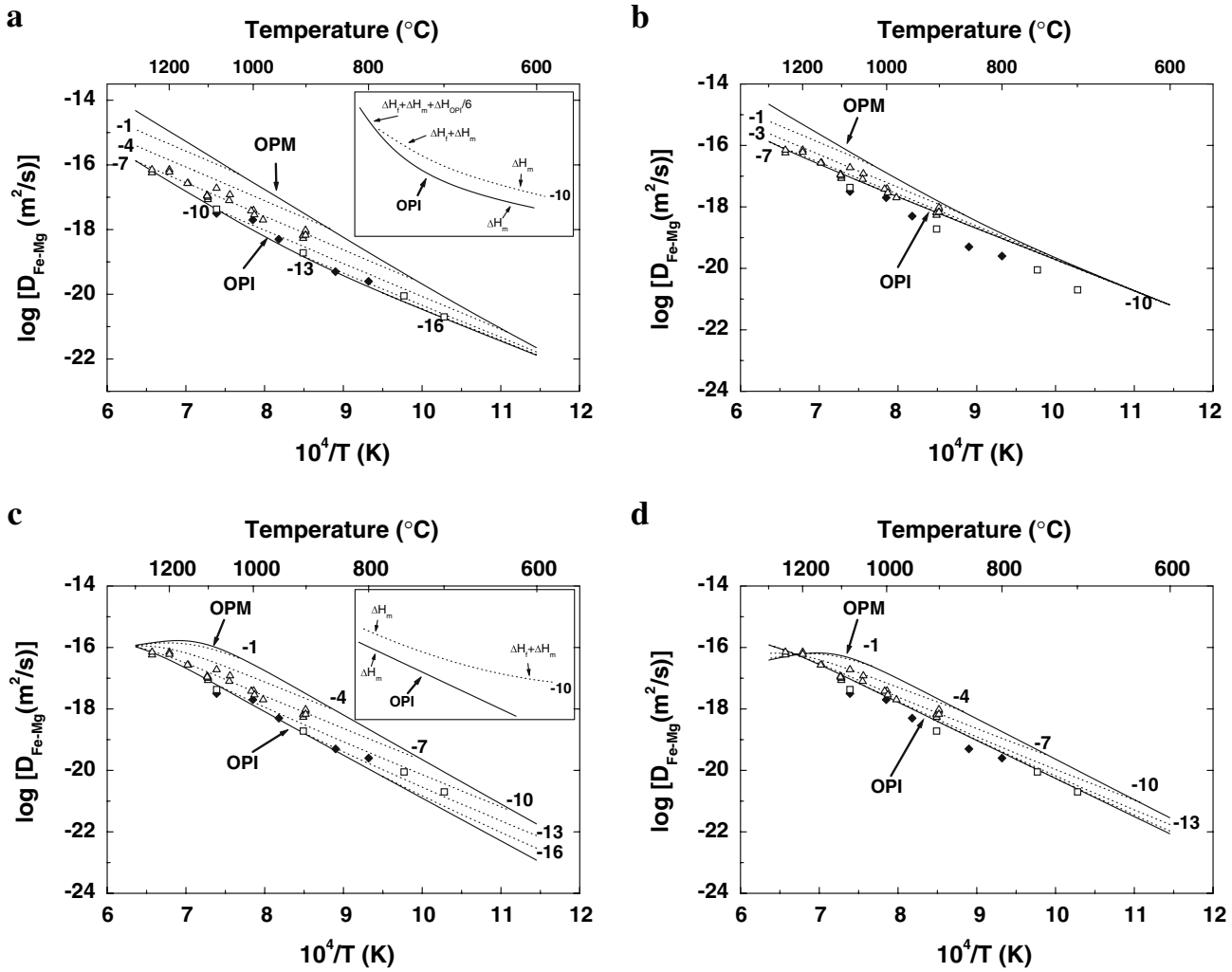


**Fig. 6** Calculated diffusion coefficients of Fe–Mg in natural olivine using (1) the calculated averaged jump frequency and (2) point defect concentrations for two different trivalent impurity concentrations for each model, in comparison with experimental data obtained along [001]. **a** 5 ppm and **b** 100 ppm for case NS-Ip; **c** 20 ppm and **d** 100 ppm for case TD-Ip. The diffusion data are measured at an $fO_2$ of $10^{-7}$ Pa (*open triangles*), $10^{-10}$ Pa (*solid diamonds*), and $10^{-12}$ Pa (*open squares*). The dotted lines are calculated diffusion coefficients at a constant $fO_2$, which is indicated on each line. The *solid lines* are calculated diffusion coefficients for an $fO_2(T)$ defined by the OPM or OPI reaction marking the stability of olivine. In the inset of (**a**), the quantities defining the slopes of different lines in these plots are clarified in an exaggerated manner, where: $\Delta H_f \equiv$ formation enthalpy of a single vacancy in the TaMED regime, $\Delta H_m \equiv$ migration enthalpy for diffusion and $\Delta H_{OPI}$ or $\Delta H_{OPM}$ (not shown) $\equiv$ enthalpy change of the reaction marking the lower or upper stability of olivine, respectively

below this critical $fO_2$. In the case of NS-Ip, for 5 ppm concentration of $IP3^{\bullet}_{Me}$ the change in the disorder type occurs around an $fO_2$ of $10^{-10}$ Pa, consistent with the experimental data. However, because of the small positive defect formation enthalpy the activation energy becomes slightly smaller within the lower temperature PED regime whereas a fit to the experimental diffusion data at lower temp gives a *steeper* slope than that predicted by the model. Therefore, the experimental data at lower temperatures are not so well reproduced by the model. In comparison, for a change in the disorder type at the same $fO_2$ of $10^{-10}$ Pa, the model of TD02 (case TD-Ip) requires an impurity concentration of 100 ppm but then the slope of the lower temperature diffusion data is not well reproduced. Instead, if the impurity content for the calculation is reduced to ~20 ppm, then an excellent fit is obtained to the slope of the data at lower temperatures, but the transition from TaMED to PED mechanism is still not complete and some $fO_2$ dependence remains between $10^{-10}$ and $10^{-12}$ Pa. To clarify this, diffusion data at still lower $fO_2$ would be required. As might have been anticipated from the uncertainties related to temperature dependence of defect formation according to the two models and the nature of thermodynamic non-ideality, it is difficult to choose unequivocally between the models. However, the match with the larger lower temperature activation energy and consistency with independently obtained defect migration enthalpies (Kohlstedt and Mackwell 1998) indicates that the TD02 model may be more realistic.

It may appear that the inability to choose definitively between the two available point defect models and datasets renders the entire analysis of diffusion data based on point defects futile. We would like to point out that fortuitously, the two models represent two extremes in the nature of temperature dependence of point defect concentrations. In that regard, evaluating these has provided us with one robust and very significant conclusion—irrespective of the validity of the models, our diffusion data (Part - I) excludes the possibility that the enthalpy of vacancy formation is significantly greater than 15 kJ/mol or less than –70 kJ/mol. Indeed, –90 kJ/mol, the slope of the boundary of olivine stability, is the absolute lower limit permitted by the diffusion data—for defect formation energies lower than that, one would obtain PED diffusion at higher temperatures and TaMED behavior at lower temperatures! These possibilities of defect formation energies being either positive or negative, with magnitudes on the order of tens of kilojoules per mole is a characteristic of the TaMED regime and is substantially different from the several hundreds of kilojoules per mole of defect formation energy, always positive, expected in the intrinsic regime (e.g., Brodholt 1997). This is the robust and general conclusion likely to be valid for any silicate material.

Finally, before concluding this section, a comment is in order about the *increase* in activation energy at lower temperatures according to the TD02 model for the following two reasons: (1) in the standard scheme of classification of diffusion mechanisms, it is expected that a transition to a lower temperature, extrinsic regime is accompanied by a *decrease* in activation energy, and (2) there may appear to be an apparent conflict with an earlier observation, that in the natural olivines the vacancy concentrations are higher than in pure (Fe,Mg)-olivine and consequently, diffusion rates are expected to be faster. The first dilemma arises because of the sign of the defect formation enthalpy in the TaMED regime according to reactions such as 5a, which is negative in this case. Therefore, on transition to the pure extrinsic regime (PED) where only the migration energy plays a role in the temperature dependence of diffusion coefficient, the activation energy actually increases. The second effect is more subtle, and illustrated in Fig. 7a. Although the activation energy in the PED regime in the presence of impurities is larger, the actual value of diffusion coefficient at any temperature is higher than it would be in a pure (Fe.Mg)-olivine at the *same* $fO_2$ within the stability field of olivine. It would appear that a steepening of the slope on an Arrhenius plot would yield slower diffusion coefficients than what one would obtain by extrapolating the higher temperature Arrhenius lines. However, we recall that the $fO_2$ at which olivine is stable drops dramatically with temperature, and therefore extrapolation of lines on an Arrhenius diagram to lower temperatures, where the corresponding $fO_2$ lies outside the stability field of olivine, is meaningless—this is seen in Fig. 7a. Lines for $fO_2$ values at which olivine is actually stable in the PED domain always lie below (dotted extensions of lines in Fig. 7a, which were calculated for an $fO_2$ buffer assuming the validity of the TaMED regime at low $fO_2$, i.e. for pure olivine) the steeper, $fO_2$ independent, impurity controlled PED diffusion line.

## General Equation to describe Fe–Mg diffusion in natural olivine

The experimental diffusion data at oxygen fugacities larger than $10^{-10}$ Pa at $P = 10^5$ Pa can be approximated by the empirical equation:

$$\log D_{\mathrm{FeMg}} = \log(D^{\circ}) - \frac{Q + (P - 10^5)\cdot \Delta V}{2.303RT} + \frac{1}{n}\log(fO_2/fO_2^{\circ}) + m \cdot X_{\mathrm{Fe}} \qquad (27)$$

where $fO_2^{\circ} = 10^{-7}$ Pa, $\Delta V = 7 \times 10^{-6}$ $m^3$ /mol (Holzapfel et al. 2007), $n \sim 6$ (point defect model, this work and Part-I), $m = 3$ (derived from data in Chakraborty 1997), and for

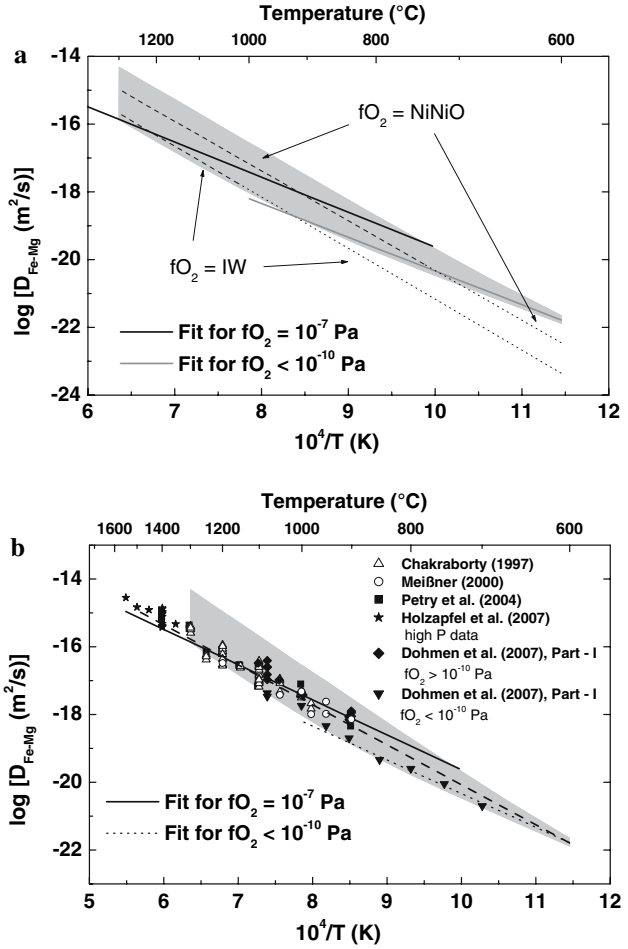


**Fig. 7** Calculated diffusion coefficients of Fe–Mg in natural olivine using the master Eqs. 27 and 28 over the entire stability field of olivine, shown as a *gray* area. **a** shows the diffusion coefficients for the complete stability field of olivine and how Eq. 27 transforms to Eq. 28 at lower temperatures over a smeared transition. *Solid line* best fit in the TaMED regime (Eq. 27), *gray line* best fit in the PED regime (Eq. 28). In addition to diffusion coefficients for a constant $fO_2$ (*solid line*) those calculated along the two buffers Ni–NiO and Fe–FeO are shown, to indicate how diffusion along a $fO_2$ buffer behaves differently from diffusion along a line of constant $fO_2$. Outside the stability field of olivine, the lines are shown as dotted extrapolations, to indicate how diffusion coefficients calculated along the lines are lower than those calculated using the PED expression, in spite of the latter having a steeper slope. In **b** calculated values are shown in comparison with 113 experimental data obtained at various $T$, $fO_2$ and $P$. It is seen that the maximum deviation for any measured data point is within 0.5 log units, relative to the two lines given by Eq. 27 (*solid*, TaMED regime) and Eq. 28 (*dotted*, PED regime). Also shown is the calculated diffusion coefficient using Eq. 29 (*dashed line*). Sources of the experimental data are given in the Legend

diffusion along [001], $Q = 201$ kJ/mol (point defect model and Part-I) and log $(D°) = -9.21$ (Part-I). The point defect calculations for natural olivine in the preceding section shows that for both models (Table 1, case 3 and 5), within the investigated range of impurity levels, there exists a temperature-$fO_2$ region where the point defect chemistry of natural olivine is almost the same as that of pure (Fe,Mg)-olivine and the point defect concentration follows an empirical equation such as Eq. 18. This is satisfied by our diffusion data at $fO_2$ above $10^{-10}$ Pa. Below an $fO_2$ of around $10^{-10}$ Pa Fe-Mg diffusion becomes almost insensitive to the $fO_2$ because of the trivalent impurities. The activation energy then resembles the migration energy and the following empirical equation can be used to calculate FeMg diffusion coefficients for olivine:

$$\log D_{\mathrm{FeMg}} = \log(D^\circ) - \frac{Q + (P - 10^5)\cdot \Delta V}{2.303RT} + 3X_{\mathrm{Fe}} \qquad (28)$$

where $Q = 220$ kJ/mol, $\Delta V = 7 \times 10^{-6}$ m$^3$ /mol, $P$ is in Pa and log $(D°) = -8.91$, obtained by fitting all data collected at $fO_2$ equal to or below $10^{-10}$ Pa in Part-I. For diffusion along [100] and [010], one needs to simply subtract log 6 from the above Eqs. (27 and 28).

Figure 7b shows a comparison of a total of 113 experimental determination of diffusion coefficients (see figure caption for sources), all normalized to a pressure of $10^5$ Pa, $fO_2 = 10^{-7}$ Pa and a composition of $Fo_{90}$, to lines calculated according to the above relationships. It is seen that the equations provide an excellent description of the experimental data and the maximum deviation of any measured data point from the calculated lines, over the entire range of determinations of the various studies, is less than half an order of magnitude (0.5 log units).

Also shown for comparison is a line given by the relation

$$\log D_{\mathrm{FeMg}} = \log(D^\circ) - \frac{Q + (P - 10^5)\cdot \Delta V}{2.303 \cdot R \cdot T} + 3 \cdot X_{\mathrm{Fe}} \qquad (29)$$

which uses the activation energy and pre-exponential factor determined by Chakraborty (1997) by fitting only a small subset of data discussed in Part-I, i.e., $Q = 226$ kJ/mol, $D° = 5.38\ 10^{-9}$ m$^2$ /s i.e. log $D° = -8.27$ and $\Delta V = 7 \times 10^{-6}$ m$^3$ /mol. It is seen that fortuitously, this relation is a compromise between (27) and (28), and can be used as a single relation to calculate $D_{\mathrm{Fe–Mg}}$ in olivine over the entire stability field of olivine (i.e., high as well as low $fO_2$ and temperature), albeit with higher deviation from the measured data points (maximum deviation is 0.5 log units for $T < 900$ °C). Equations 27 and 28 are firmly rooted in point defect chemistry and diffusion mechanisms and describe the data more accurately, Eq. 29 provides a single simplified equation for the entire range of stability of olivine that can be used in approximate modeling work.

Figure 7a and b show how the $fO_2$ dependence observed at higher temperatures disappears at lower temperatures, illustrated here for a specific concentration of $IP3^{\bullet}_{\mathrm{Me}}$ over a

transitional region, as the transition occurs from the TaMED to the PED mechanism of diffusion. On Fig. 7a, the line for any given $fO_2$ is drawn over the range of temperature where olivine is stable at that particular $fO_2$. Also shown for comparison are lines showing how diffusion coefficients change along oxygen fugacity buffers, rather than at constant oxygen fugacity, to highlight the difference in diffusion behavior with changing temperature under these two circumstances.

A consequence of the vacancy concentration in natural olivine becoming constant and independent of $fO_2$ below a critical oxygen fugacity is that the diffusion of other cations like Ni, Ca, Mn and Cr would become insensitive to $fO_2$ below this critical value in an exactly analogous manner. Other processes like electrical conductivity controlled by the concentration of electron holes ($Fe^{3+}$) (e.g., Wannamaker and Duba 1993) would still depend on $fO_2$, but the trivalent impurities on the metal site would decrease the conductivity relative to that in pure olivine.

## Summary of conclusions

The main conclusions of this work may be summarized as follows:

1. In spite of different sources of uncertainties in the point defect models and experimental data of NS83 and TD02, calculated concentrations of vacancies on octahedral sites of pure (Fe,Mg)-olivines as a function of composition and oxygen fugacity at the experimental temperature range are fairly tightly constrained to within 0.4 log units. These concentrations, at a temperature of about 1,100 °C, are on the order of 100 ppm (in atomic formula units) for olivines of intermediate compositions.
2. The strong compositional dependency of point defect concentrations and measured ''equilibrium constants'' ($K_x$, as defined in this work) by NS83 and TD02 require the mixing of vacancies on the octahedral sites to be highly non-ideal. The form of this compositional dependence is well reproduced by a ternary simple mixture model in spite of several simplifying assumptions.
3. There is considerable uncertainty in the temperature dependency of the defect forming reactions observed in both studies, mainly because of the narrow temperature range over which experiments were carried out. Most notably, the defect forming enthalpies ($\Delta H_f$) of a single octahedral vacancy in this TaMED regime are close to zero with a maximum permissible value of 15 kJ/mol for the data and model of NS83, whereas it is negative and higher in magnitude, ~ –66 kJ/mol, according to the data and model of TD02. These have important consequences for the behavior of diffusion data as a function of temperature. We have calculated and presented plots of vacancy concentrations as a function of temperature and oxygen fugacity according to both models, over the entire stability field of olivine, to highlight the similarities as well as differences between the two studies (NS83 and TD02).
4. For natural olivines, it is necessary to take into account the concentration of aliovalent trace elements (e.g., Al, Cr) in determining the concentration of point defects and transport properties. We have developed an extension of the point defect models taking this aspect into consideration, and have presented plots to show that the concentrations of point defects and the general behavior changes dramatically when the effect of such trivalent trace elements are taken into account, particularly at low temperatures and $fO_2$. It is found that the exact structural location of these trace impurities plays a key role and needs to be determined better than is presently known.
5. We have further developed a formulation to relate measured diffusion coefficients directly to these variations of point defect concentrations. This allows us to (a) produce schemes for calculation of diffusion coefficients from point defect concentration data across the entire stability field of olivine, if diffusion data at a few conditions are available, and (b) test the two available point defect models and data, NS83 and TD02.
6. The analysis in (4) and (5) reveals that due to a transition from TaMED to PED mechanism of diffusion (Chakraborty 1997 and Appendix A), it would be expected that at lower $T$ and/or $fO_2$, the diffusion coefficients would become independent of $fO_2$ and that the observed activation energy could become higher/lower by a few tens of kJ/mol (see also Chakraborty 1997). This is exactly the behavior observed in Part I. Therefore, in combination, these two works constitute the first demonstration of a transition from TaMED to PED mechanism of diffusion in any material, and also the first unequivocal demonstration of a change of mechanism of diffusion in any silicate mineral.
7. Comparison of calculated variation of diffusion data as a function of $T$ and $fO_2$ with measured data shows that (1) the transition from $fO_2$ dependent to $fO_2$ independent diffusion behavior occurs in a manner more consistent with the NS83 model, whereas (2) the change of activation energy of diffusion at lower temperatures to *higher* values is more consistent with the TD02 model. The inferred migration enthalpy of ~ 260 kJ/mol from the latter, and its agreement with the independent estimates of Kohlstedt and Mackwell (1998), suggests that at the present time the data and

model of TD02 is slightly preferable. The corresponding enthalpy for the formation of a single vacancy is ~ –66 kJ/mol, the negative sign being the reason behind the steepening of the slope on the Arrhenius plot at lower temperatures.

8. The prediction of the TD02 model is that the transition from $fO_2$ dependent to $fO_2$ independent diffusion behavior should occur over a larger range than that covered currently by experimental data—future experiments at lower temperatures and oxygen fugacities may clarify/constrain the model further. An important characteristic of the TaMED to PED transition, unlike the classical intrinsic–extrinsic transitions that produces a kink on an Arrhenius diagram, is that it is smeared in an Arrhenius plot, i.e., takes place over a range of $T$ (up to several hundred degrees) and $fO_2$ (several log units). Consequently, slopes of lines may be gently curved, leading to difficulties in the measurement and characterization of this behavior.
9. Considering the point defect based diffusion mechanisms and the diffusion data, we have provided equations for the calculation of FeMg diffusion coefficients over the entire stability field of olivine as functions of $P$, $T$, $X_{Fe}$, $fO_2$. One problem in formulating such a relationship is the aspect noted under (8) and illustrated in Figs. 4, 6 and 7—the behavior of diffusion coefficients is described by curved, rather than straight, lines on an Arrhenius diagram. As a compromise, we have produced piecemeal straight line Arrhenius relationships to describe the diffusion data—Eq. 27 for the TaMED region (approximately above 900 °C and $fO_2 = 10^{-10}$ Pa), Eq. 28 for the PED regime (lower $T$ or $fO_2$) and Eq. 29 for a compromise straight line that can be used over the entire stability field of olivine, but with larger errors (underestimates $D$ at higher $T$ and overestimates $D$ at lower $T$). Eqs. 27 and 28 in combination are found to reproduce all experimental measurements from our laboratories (113 data points) within 0.5 log units.
10. The transition from TaMED to PED found here for olivines is likely to be common in other ferromagnesian silicates and oxides. Two key characteristics of diffusion in the TaMED regime are defect formation enthalpies on the order of tens of kilo joules per mole (as opposed to several hundred kilojoules per mole for intrinsic, thermal defect formation), and the fact that these energies can be either positive or negative. As we have seen here, these features combined with the smeared nature of the transition render conventional intrinsic/extrinsic transition (= kink in an Arrhenius plot) based considerations of diffusion in silicate and oxide minerals too simplistic. Interpretation of experimental diffusion data as well as conception and execution of atomistic computer models need to consider these aspects in future work.

**Acknowledgements** We thank the German Science Foundation (DFG) for generously supporting this work by covering the entire salary of the first author. This support was obtained in part within the interdisciplinary program SFB 526 (Rheology of the Earth). We thank David Kohlstedt, Jibamitra Ganguly and John Farver for very constructive and helpful reviews.

## Appendix A: Disorder and diffusion mechanisms in Fe-bearing silicates: terminology

### Intrinsic disorder/diffusion

A crystal is intrinsically disordered, if the concentrations of the majority point defects at a given composition depend only on $P$ and $T$ (Schmalzried 1981). Diffusion in such crystals occurs with a high activation energy that is the sum of the intrinsic defect formation (always positive, several 100 kJ/mol) and migration energy. Relevant only at high temperatures and very pure crystals.

### Pure extrinsic disorder/diffusion (PED)

Strictly defined (Schmalzried 1981), a crystal of a given major element composition has extrinsic disorder if the majority point defects are controlled by the potential of some chemical components in addition to $P$ and $T$. Diffusion in such crystals occurs with a relatively low activation energy, corresponding to the migration energy only. Relevant at relatively low temperatures and/or oxygen fugacities; the higher the impurity content, the higher the temperature of onset of diffusion by this mechanism.

This definition of extrinsic disorder is only useful if the crystal is an open system and concentrations of trace elements can be controlled by chemical activities imposed by the external surroundings. If the crystal is a closed system (e.g., at low temperatures where kinetics inhibits interaction with a surrounding reservoir) on timescales of interest, then the majority point defects may still be determined by the concentration of aliovalent impurities already incorporated into the crystal at some stage of its history. This constant concentration is determined, of course, by the chemical potential of the impurity at that stage e.g. typically during formation of the crystal. A well known example is Sr doped NaCl (e.g., see discussion in Lasaga 1998). Here the extrinsic disorder is defined by the fixed concentration of Sr in NaCl. For the present paper such a situation is also considered as pure extrinsic, because the activation energy of diffusion does not have any contribution from a formation energy.

Transition metal extrinsic disorder/diffusion (TaMED)

This is a term introduced by Chakraborty (1997) in his study of olivines to describe an intermediate situation that arises in transition metal (most importantly Fe) bearing silicates in general. Here majority point defect concentrations in a crystal of a given composition depend on $P$, $T$ and chemical potential of a particular kind—$fO_2$, similar to the PED case. Analogous to the intrinsic regime, however, diffusion occurs with an activation energy that is a sum of a formation energy (but a different one—it is only several tens of kJ/mol, positive or negative) and a migration energy. The formation energy in this context refers to the free energy change / enthalpy change of reactions such as those denoted by Eqs. 5a and 5b in this work, rather than the thermal defect forming reactions. This mechanism is relevant at intermediate temperatures and oxygen fugacities unless the defect formation energies are unusually negative, see text for more details.

An example is the case being studied in this work where the majority point defects $V_{Fe}$ and $Fe^{3+}$ are controlled by $fO_2$ and $a(SiO_2)$ and their concentrations change with temperature at a constant oxygen fugacity.

## Appendix B: A thermodynamic mixing model considering majority point defects

A standard thermodynamic ternary mixing model is applied for three chemical species on the octahedral metal site: $V''_{Me}$ , $Fe^{x}_{Me}$ , $Mg^{x}_{Me}$. The general expression for the activity coefficient, within the framework of a simple mixture formalism, of a species $i$ in a ternary system with three symmetric binary interactions is (e.g., Ganguly and Saxena 1987):

$$RT\ln(\gamma_i) = \sum_{j\neq i}\left\{W_{ij}\cdot X_j^2 + X_jX_k\left[W_{ij}+W_{ik}-W_{jk}-C_{ijk}(1-2X_i)\right]\right\} \quad (30)$$

where $X_i$ denotes the mole fraction of species i on the metal site (note that for $Fe^{x}_{Me}$ the mole fraction is related to the a.f.u. of olivine $X_{Fe} = [Fe^{x}_{Me}]/2$), $W_{ij}$ is the binary interaction parameter, and $C_{ijk}$ is the ternary interaction parameter. Since the mole fraction of the vacancies on the metal site is small, it can be set to zero and to further simplify the analysis it is assumed that $W_{VMe} := |W_{VMg}| = |W_{VFe}| >> |W_{FeMg}|$. Considering also that $X_{Mg} = 1 - X_{Fe}$, the final equation for the activity coefficient of the metal vacancies is:

$$RT\ln(\gamma_{V''_{Me}}) = W_{VMe} + 2(W_{VMe}-C)\cdot X_{Fe} - 2(W_{VMe}-C)\cdot X_{Fe}^2 \quad (31)$$

This can be written more simply by defining an average interaction parameter, $\bar{W}_{VMe} = 2(W_{VMe} - C)$. An analogous equation can be derived for $Fe^{3+}$ on the metal site if the interaction with the vacancies can be ignored as it is typically done. Note that for a constant olivine composition, the activity coefficient in Eq. 31 is a constant and Henry's law is fulfilled as it is typically assumed for dilute constituents like point defects. Furthermore, with the above assumptions an ideal behavior is obtained for the regular structural units (ignoring the interaction between Fe and Mg). The expression may be further simplified by ignoring the ternary interaction parameter, as is often done. In that case, the expression for activity coefficient becomes a simple polynomial in $X_{Fe}$ with one interaction parameter,

$$RT\ln(\gamma_{V''_{Me}}) = W_{VMe}\left[1 + 2\cdot X_{Fe} - 2\cdot X_{Fe}^2\right].$$

Incorporation of non-ideality of the point defects into the mass action laws for point defect formation reactions, e.g., for reaction 5a (Eq. 6a), yields

$$\ln(K_{5a}) = \ln\left(\frac{\left[V''_{Me}\right]^2\cdot\left[Fe^{\bullet}_{Me}\right]^4}{(X_{Fe})^4\cdot a_{SiO_2}\cdot f_{O_2}}\right) + \ln\left(\gamma^2_{V''_{Me}}\cdot\gamma^4_{Fe^{\bullet}_{Me}}\right) \quad (32)$$

connecting the point defect concentrations, $fO_2$, $a(SiO_2)$ and the equilibrium constant (Compare with Eq. 7a).

Defining $\ln(K^{\gamma}_{5a}) = \ln\left(\gamma^2_{V''_{Me}}\cdot\gamma^4_{Fe^{\bullet}_{Me}}\right)$ and $\ln(K'_{5a}) = \ln(K_{5a}) - \ln(K^{\gamma}_{5a})$, Eq. 7a is obtained from the above equation. Using now Eq. 31 the $K_x$ of Reaction 5a can be derived as an explicit function of $X_{Fe}$:

$$\ln(K_{x(5a)}) = \ln(K_{5a}) - \frac{2W_{VMe}+4W_{Fe^{3+}Me}}{RT} - \frac{2\bar{W}_{VMe}+4\bar{W}_{Fe^{3+}Me}}{RT}X_{Fe} + \frac{2\bar{W}_{VMe}+4\bar{W}_{Fe^{3+}Me}}{RT}X_{Fe}^2 \quad (33)$$

For positive values of the interaction parameters, the form of compositional dependence of the experimentally determined $K_x$ (Fig. 1) are approximately reproduced showing the first order validity of the simplified mixing model. Within the scope of validity of such relationships, it is evident that a strong change in the compositional dependence of $K_x$ over a small temperature interval (70 °C) is impossible, which means that in a diagram such as Fig. 1 the data at different temperatures should mainly be shifted by a constant value independent of the fayalite content.

## Appendix C: stability field of olivine as function of T and $fO_2$

The stability field of Mg-rich olivine at $10^5$ Pa with respect to $fO_2$ is defined by the following two reactions:

$$Fe_2SiO_4(ol) = FeSiO_3(opx) + Fe(m) + 0.5O_2(g) \quad (34)$$

$$6Fe_2SiO_4(ol) + O_2(g) = 6FeSiO_3(opx) + 2Fe_3O_4(mf), \quad (35)$$

where the first reaction defines the phase boundary of olivine to low oxygen fugacities and the second marks the boundary to oxidizing conditions. From the corresponding mass action laws it follows:

$$\log(fO_2)_{OPI} = 2\log(K_{34}) + 2\log(a^{ol}_{Fe_2SiO_4}) - 2\log(a^{opx}_{FeSiO_3}) - 2\log(a^{m}_{Fe}) \quad (36)$$

$$\log(fO_2)_{OPM} = -\log(K_{35}) - 6\cdot\log(a^{ol}_{Fe_2SiO_4}) + 6\cdot\log(a^{opx}_{FeSiO_3}) + 2\cdot\log(a^{mf}_{Fe_3O_4}) \quad (37)$$

For a given forsterite content in olivine the activity of $Fe_3O_4$ and $FeSiO_3$ are defined by the Fe–Mg exchange equilibrium between ol/mf and ol/opx, respectively. The solubility of Mg and Si into metal can be neglected. We have used the self consistent data set of Fabrichnaya et al. (2004) for the system Fe, Mg, Al, Si and O to calculate the stability field of pure olivine with respect to $fO_2$ (Fig. 8). The calculations were performed using the software ChemSage (GTT Technologies). From the calculations we have obtained an empirical relation that describes log $fO_2$ along the two phase boundaries for a $Fo_{90}$ olivine in $T$ - $fO_2$ space:

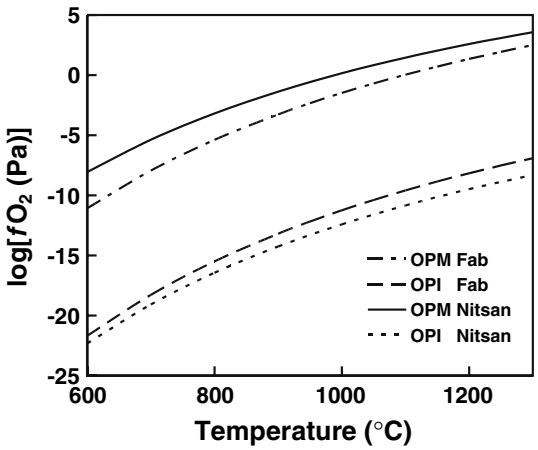


**Fig. 8** Stability field of olivine of $Fo_{90}$ composition with respect to $fO_2$ between 600 and 1,300 °C calculated using the data set of Fabrichnaya et al. (2004) shown in comparison to that of Nitsan (1974)

$$\log(fO_2)_{OPI} = 11.5203 - 2.8892\cdot\frac{10^4}{T(K)} \quad (38)$$

$$\log(fO_2)_{OPM} = 19.409 - 2.6606\cdot\frac{10^4}{T(K)} \quad (39)$$

The calculated stability field in Fig. 8 is shown in comparison to the results of Nitsan (1974). The stability field is up to one log unit of $fO_2$ smaller compared to the calculation of Nitsan (1974), mainly for two reasons. First, recent revision of the thermodynamic data of the end members yields smaller and higher values for log $K_{34}$ and log $K_{35}$, respectively, and second, the dilution effect of $Fe_3O_4$ into magnesioferrite had not been considered by Nitsan (1974). For natural olivine the presence of trace elements like Cr, Al, Mn or H is not expected to significantly affect the stability field, but Ni has to be considered because it dissolves in considerable amounts into the metal phase at relevant $fO_2$ and lowers thereby its activity, which broadens the stability field of metal and lowers that of olivine (Matas et al. 2000). Matas et al. (2000) have explored the effect of dissolution of Ni in metal in modifying the stability field of olivine. They find that the stability fields are reduced by up to 1.5 log units (at about 600 °C) for the lower boundary due to this effect. This should be considered in using our Fig. 8.

In the calculations in this paper we have used the above relationships to locate the boundaries of the stability fields of olivine.

## References

Bai Q, Kohlstedt DL (1993) Effects of chemical environment on the solubility and incorporation mechanism for hydrogen in olivine. Phys Chem Miner 19:460–471

Barkmann T, Cemic L (1996) Impedance spectroscopy and defect chemistry of fayalite. Phys Chem Miner 23:186–192

Barrer RM, Bartholomew RF, Rees LVC (1963) Ion exchange in porous crystals Part II. The relationship between self- and exchange-diffusion coefficients. J Phys Chem Solids 24:309–317

Brodholt J (1997) Ab initio calculations on point defects in forsterite (Mg2SiO4) and implications for diffusion and creep. Am Miner 82:1049–1053

Chakraborty S (1997) Rates and mechanisms of Fe–Mg interdiffusion in olivine at 980 –1,300 °C. J Geophys Res 102(B6):12317–12331

Dieckmann R, Schmalzried H (1975) Point defects in oxide solid solutions (III) mobilities of cations and vacancies in (Co, Ni)O- and (Co, Mg)O-solid solutions and the calculation of correlation factors. Ber Bunsenges Phys Chem 79:1108–1115

Dohmen R, Becker H-W, Chakraborty S (2002) Si and O diffusion in olivine and implications for characterizing plastic flow in the mantle. Geophys Res Lett 29, doi:10.1029/2002GL015480

Dohmen R, Becker H-W, Chakraborty S (2007) Fe–Mg diffusion in olivine I: Experimental determination between 700 and 1,200°C as a function of composition, crystal orientation and oxygen fugacity. Phys Chem Miner (this volume)

Fabrichnaya OB, Saxena SK, Richet P, Westrum EF (2004) Thermodynamic data, models, and phase diagrams in multicomponent oxide systems. Springer, Berlin, 198p

Ganguly J, Saxena SK (1987) Mixtures and mineral reactions. Springer, Berlin

Hier-Majumder S, Anderson IM, Kohlstedt DL (2005) Influence of protons on Fe–Mg interdiffusion in olivine. J Geophys Res 110:B02202. doi: 10.1029/2004JB003292

Hillert M, Selleby M, Sundman B (1996) A reassessment of the nonstoichiometry of fayalite. Phys Chem Miner 23:387–390

Hirsch LM, Shankland TJ (1991) Determination of defect equilibria in minerals. J Geophys Res 96:377–384

Holzapfel C, Chakraborty S, Rubie DC, Frost DJ (2007) Effect of pressure on Fe-Mg, Ni and Mn diffusion in $(Fe_xMg_{1-x})_2SiO_4$ olivine. Phys Earth Planet Int (accepted)

Kohlstedt DL, Mackwell SJ (1998) Diffusion of hydrogen and intrinsic point defects in olivine, Zeitschr. Phys Chem 207:147–162

Lasaga AC (1979) Multicomponent exchange and diffusion in silicates. Geochim Cosmochim Acta 43:455–469

Lasaga AC (1998) Kinetic theory in the earth sciences. Princeton University Press, Princeton, 811p

Manning JR (1968) Diffusion kinetics for atoms in crystals. Van Nostrand, Princeton, 257 pp

Matas J, Ricard Y, Lemelle L, Guyot F (2000) An improved thermodynamic model of metal-olivine-pyroxene stability domains. Contrib Miner Petrol 140:73–83

Meißner (2000) Messung von kurzen Konzentrationsprofilen mit Hilfe der analytischen Transmissionselektronenmikroskopie (TEM-EDX) am Beispiel der Bestimmung von Diffusionskoeffizienten für Mg-Fe Interdiffusion in Olivin. Dissertation, Bayreuth

Nakamura A, Schmalzried H (1983) On the nonstoichiometry and point defects of olivine. Phys Chem Miner 10:27–37

Nakamura A, Schmalzried H (1984) On the $Fe^{2+}$-$Mg^{2+}$-interdiffusion in olivine (II). Ber Bunsenges Phys Chem 88:140–145

Nitsan U (1974) Stability field of olivine with respect to oxidation and reduction. J Geophys Res 79:706–711

Petry C, Chakraborty S, Palme H (2004) Experimental determination of Ni diffusion coefficients in olivine and their dependence on temperature, composition, oxygen fugacity, and crystallographic orientation. Geochim Cosmochim Acta 68:4179–4188

Sato (1986) High temperature a.c. electrical properties of olivine single crystal with varying oxygen partial pressure: implications for the point defect chemistry. Phys Earth Planet Inter 41:269–282

Schmalzried H (1983) Thermodynamics of compounds with narrow ranges of stoichiometry. Ber Bunsen Ges Phys Chem 87:726–733

Simons B (1986) Temperatur- und Druckabhängigkeit der Fehlstellenkonzentration der Olivine und Magnesiowüstite. Habilitation thesis, University of Kiel, Kiel, 175p

Stalder R, Klemme S, Ludwig T, Skogby H (2005) Hydrogen incorporation in orthopyroxene: interaction of different trivalent cations. Contr Miner Petrol, doi: 10.1007/s00410-005-0037-4

Tsai T-L, Dieckmann R (2002) Variation of the oxygen content and point defects in olivines, $(Fe_xMg_{1-x})_2SiO_4$, $0.2 \leq x \leq 1.0$. Phys Chem Minerals 29:680–694

Wannamaker BJ, Duba AG (1993) Electrical conductivity of San Carlos olivine along [100] under oxygen- and pyroxene-buffered conditions and implications for defect equilibria. J Geophys Res 98(B1):489–500